Inputs and processes affecting the distribution of particulate iron in the North Atlantic along the GEOVIDE (GEOTRACES GA01) section

Arthur Gourain[1,2], Hélène Planquette[1], Marie Cheize[1,3], Nolwenn Lemaitre[1,4], Jan-Lukas Menzel Barraqueta[5], Rachel Shelley[1, 6], Pascale Lherminier[7] and Géraldine Sarthou[1]

1-UMR 6539/LEMAR/IUEM, Technopôle Brest Iroise, Place Nicolas Copernic, 29280 Plouzané, France
2- now at Ocean Sciences Department, School of Environmental Sciences, University of Liverpool, Liverpool, L69 3GP, United Kingdom
3- now at Ifremer, Centre de Brest, Géosciences Marines, Laboratoire des Cycles Géochimiques (LCG), 29280 Plouzané, France
4- now at Department of Earth Sciences, Institute of Geochemistry and Petrology, ETH-Zürich, Zürich, Switzerland
5- GEOMAR, Helmholtz Centre for Ocean Research Kiel, Wischhofstraße 1-3, 24148 Kiel, Germany
6- now at Earth, Ocean and Atmospheric Science, Florida State University, Tallahassee, Florida, 32310, USA
7- Ifremer, LPO, UMR 6523 CNRS/Ifremer/IRD/UBO, Ifremer Centre de Brest, CS 10070, Plouzané, France

Correspondence to: helene.planquette@univ-brest.fr

Abstract

The GEOVIDE cruise (May-June 2014, R/V Pourquoi Pas?) aimed to provide a better understanding on trace metal biogeochemical cycles in the North Atlantic. As particles play a key role in the global biogeochemical cycle of trace elements in the ocean, we discuss the distribution of particulate iron (PFe), in light of particulate aluminium (PAl), manganese (PMn) and phosphorus (PP) distributions. Overall, 32 full vertical profiles were collected for trace metal analyses, representing more than 500 samples. This resolution provides a solid basis for assessing concentration distributions, elemental ratios, size-fractionation, or adsorptive scavenging processes in key areas of the thermohaline circulation. Total particulate iron (PFe) concentrations ranged from as low as 9 pmol L^{-1} in surface Labrador Sea waters to 304 nmol L^{-1} near the Iberian margin, while median PFe concentrations of 1.15 nmol L^{-1} were measured over the sub-euphotic ocean interior.

Within the Iberian Abyssal Plain, ratio of PFe over particulate aluminium (PAl) is identical to the continental crust ratio (0.21), indicating the important influence of crustal particles in the water column. Overall, the lithogenic component explained more than 87% of PFe variance along the section. Within the Irminger and Labrador basins, the formation of biogenic particles led to an increase of the PFe/PAl ratio (up to 0.7 mol mol-^{1}) compared to the continental crust ratio (0.21 mol mol^{-1}). Margins provide important quantities of particulate trace elements (up to 10 nmol L^{-1} of PFe) to the open ocean, and in the case of the Iberian margin, advection of

PFe was visible more than 250km away from the margin. Additionally, several benthic nepheloid layers spreading over 200m above the seafloor were encountered along the transect, especially in the Icelandic, Irminger and Labrador basins, delivering particles with high PFe content, up to 89 nmol L^{-1} of PFe. Finally, remineralisation processes are also discussed, and showed different patterns among basins and elements.

1. Introduction

Particles play a key role in the ocean where they drive the residence time of most elements (Jeandel et al., 2015), and strongly influence the global biogeochemistry of macro and micro-nutrients including iron (Milne et al., 2017). In the surface ocean, biological activity produces biogenic suspended matter through planktonic organisms, while atmospheric deposition (Baker et al., 2013; Jickells et al., 2005), riverine discharge (Aguilar-Islas et al., 2013; Berger et al., 2008; Ussher et al., 2004) or ice-melting (Hawkings et al., 2014; Lannuzel et al., 2011, 2014) bring mostly lithogenic derived particles to surface waters. These particulate inputs highly vary, both spatially and seasonally, around the world's oceans. At depth, benthic and shelf sediment resuspension (e.g. Aguilar-Islas et al., 2013; Cullen et al., 2009; Elrod et al., 2004; Fitzwater et al., 2000; Hwang et al., 2010; Lam et al., 2015; Lam and Bishop, 2008; McCave and Hall, 2002), and hydrothermal activity (Elderfield and Schultz, 1996; Lam et al., 2012; Tagliabue et al., 2010, 2017; Trefry et al., 1985), provides important amounts of particles to the water column. Moreover, authigenic particles can be produced *in-situ* by aggregation of colloids (Bergquist et al., 2007) or oxidation processes (Bishop and Fleisher, 1987; Collier and Edmond, 1984). Thus, oceanic particles result from a complex combination of these different sources and processes (Lam et al., 2015).

Particles represent the main part of the total iron pool in the upper water column (Radic et al., 2011), and strongly interact with the dissolved pool (e.g. Ellwood et al., 2014). Indeed, dissolved iron can be scavenged onto particles (Gerringa et al., 2015; Rijkenberg et al., 2014), incorporated into biogenic particles (Berger et al., 2008) or produced by remineralisation of particles (Dehairs et al., 2008; Sarthou et al., 2008). Interestingly, the concept of "reversible scavenging" (i.e. release at depth of dissolved iron previously scavenged onto particles) has been advocated recently (Dutay et al., 2015; Jeandel and Oelkers, 2015; Labatut et al., 2014), while other studies reveal distinct dissolution processes (e.g. Oelkers et al., 2012; Cheize et al., submitted to Chemical Geology). Slow dissolution of particulate iron at margins has also been evoked as a continuous fertilizer of primary production and should be considered as a source of dissolved iron (e.g. Jeandel et al., 2011; Jeandel and Oelkers, 2015; Lam and Bishop, 2008). Within or below the mixed layer, the rates of regeneration processes can also impact the bioavailable pool of iron, among other trace metals (e.g. Ellwood et al., 2014; Nuester et al., 2014). However, the rates of these processes are not yet fully constrained. The study of particulate iron is thus essential to better constrain the global biogeochemical cycle of iron in the ocean. This subject received a growing interest over the last 10 years in particular (e.g. Bishop and Biscaye, 1982; Collier and Edmond, 1984; Frew et al., 2006; Lam et al., 2012; Milne et al., 2017; Planquette et al., 2011, 2013; Sherrell et al., 1998) and, to our knowledge, only two have been performed at an ocean-wide scale and published so far: the GA03 GEOTRACES North Atlantic Zonal Transect (Lam et al., 2015; Ohnemus and Lam, 2015) and the GP16 GEOTRACES Pacific Transect (Lam et al., 2017; Lee et al., 2017).

In this context, this paper presents the particulate iron distribution in the North Atlantic Ocean, along the GEOTRACES GA01 section (GEOVIDE), and discusses the various sources and processes affecting its distribution, using particulate aluminium, phosphorus or manganese.

2. Methods

2.1. Study area

Particulate samples were collected at 32 stations during the GEOVIDE (GEOTRACES GA01 section) cruise between May and June 2014 aboard the R/V *Pourquoi Pas?* in the North Atlantic. The sampling spanned several biogeochemical provinces (Figure 1) that first comprised the Iberian margin (IM, Stations 2, 1 and 4), the Iberian Abyssal Plain (IAP, Stations 11 to 17), the Western European Basin (WEB, Station 19 to Station 29) and the Icelandic Basin (IcB, Stations 32 to 36). Then, samples were collected above the Reykjanes Ridge (RR, Station 38), in the Irminger Basin (IrB, Stations 40 to 60), close to the Greenland shelf (GS, Stations 53 and 61), the Labrador Basin (LB, Stations 63 to 77) and finally close the Newfoundland shelf (NS, Station 78) (Figure 1). The North Atlantic is characterized by a complex circulation (briefly described in section 2.1 and in detail by Zunino et al. (2017) and García-Ibáñez et al. (2015) and is one of the most productive regions of the global ocean (Martin et al., 1993; Sanders et al., 2014), with a complex phytoplankton community structure composed of diverse taxa (Tonnard et al., in prep.).

2.2. Sampling

Samples were collected using the French GEOTRACES clean rosette, equipped with twenty-two 12L GO-FLO bottles (two bottles were leaking and were never deployed during the cruise). GO-FLO bottles (General Oceanics) were initially cleaned in the home laboratory (LEMAR) following the GEOTRACES procedures (Cutter and Bruland, 2012). The rosette was deployed on a 14mm Kevlar cable with a dedicated, custom-designed clean winch. Immediately after recovery, the GO-FLO bottles were individually covered at each end with plastic bags to minimize contamination. They were then transferred into a clean container (class-100) for sampling, and the filters processed under a laminar flow unit. On each cast, nutrient and/or salinity samples were taken to check potential leakage of the GO-FLO bottles.

Filters were cleaned following the GEOTRACES protocols (http://www.geotraces.org/images/Cookbook.pdf) and kept in acid-cleaned 1 L LDPE bottles (Nalgene) filled with ultrapure water (Milli-Q, resistivity of 18.2 MΩ cm) until use. All filters were 25 mm diameter in order to optimize signal over the filter blank except at the surface depth where 47 mm diameter filters mounted on acid-cleaned polysulfone filter holders (Nalgene^{TM}) were used. Prior to filtration, the GO-FLO bottles were shaken three times, as recommended in the GEOTRACES cookbook to avoid settling of particles in the lower part of the bottle. GO-FLO bottles were pressurized to <8 psi with 0.2 µm filtered dinitrogen (N_2, Air Liquide). Seawater was then filtered directly through paired filters (Pall Gelman Supor^{TM} 0.45 µm polyetersulfone, and Millipore mixed ester cellulose MF 5 µm) mounted in Swinnex polypropylene filter holders (Millipore), following Planquette and Sherrell (2012) inside the clean container. Filtration was operated until the bottle was empty or until the filter clogged; volume filtered ranged from 2 liters for surface samples to 11L within the water column.. After filtration, filter holders

were disconnected from the GO-FLO bottles and a gentle vacuum was applied using a syringe in order to remove any residual water under a laminar flow hood. Filters were then removed from the filter holders with plastic tweezers that were rinsed with Milli-Q between samples. Most of the remaining seawater was 'sipped' by capillary action, when placing the non-sampled side of the filter onto a clean 47 mm supor filter. Then, each filter pair was placed in an acid-cleaned polystyrene PetriSlides (Millipore), double bagged, and finally stored at -20°C until analysis at LEMAR. Between casts, filter holders were thoroughly rinsed with Milli-Q, placed in an acid bath (5% HCl) for 24 hours, then rinsed with Milli-Q.

At each station, process blanks were collected as follows: 2L of a deep (1000 m) and a shallow (40 m) seawater samples were first filtered through a 0.2 µm pore size capsule filter (Pall Gelman Acropak 200) mounted on the outlet of the GO-FLO bottle before to pass through the particle sampling filter, which was attached directly to the swinnex filter holder.

2.3. Analytical methods

Back in the home laboratory, sample handling was performed inside a clean room (Class 100). All solutions were prepared using ultrapure water (Milli-Q) and all plasticware had been acid-cleaned before use. Frozen filters, collected within the mixed layer depth or within nepheloid layers, were first cut in half using a ceramic blade: one filter half was dedicated to total digestion (see below), while the other half was archived at -20°C for SEM analyses or acid leaching of "labile" metals (Berger et al., 2008; to be published separately).

Filters were digested following the method described in Planquette and Sherrell (2012). Filter were placed on the inner wall of acid-clean 15mL PFA vials (Savillex^{TM}), and 2 mL of a solution containing 2.9 mol L^{-1} hydrofluoric acid (HF, suprapur grade, Merck) and 8 mol L^{-1} nitric acid (HNO_3, Ultrapur grade, Merck) was added to each vial. Vials were then closed and refluxed at 130°C on a hot plate for 4 hours. After cooling, the digest solution was evaporated at 110°C until near dryness. Then, 400 µL of concentrated HNO_3 (Ultrapur grade, Merck) was added, and the solution was re-evaporated at 110°C. Finally, the obtained residue was dissolved with 3mL of a 0.8 mol L^{-1} HNO_3 (Ultrapure grade, Merck). This archive solution was transferred to an acid cleaned 15 mL polypropylene centrifuge tube (Corning®) and stored at 4°C until analyses.

All analyses were performed on a sector field inductively coupled plasma mass spectrometer (SF-ICP-MS Element2, Thermo-Fisher Scientific). Samples were diluted by a factor of 7 on the day of analysis in acid-washed 13 mm (outer diameter) rounded bottom, polypropylene centrifuge tubes (VWR) with 0.8 mol L^{-1} HNO_3 (Ultrapur grade, Merck) spiked with 1µg L^{-1} of Indium (^{115}In) solution in order to monitor the instrument drift. Samples were introduced with a PFA-ST nebulizer connected to a quartz cyclonic spray chamber (Elemental Scientific Incorporated, Omaha, NE) via a modified SC-Fast introduction system consisting of an SC-2 autosampler, a six-port valve and a vacuum-rinsing pump. The autosampler was contained under a HEPA filtered unit (Elemental Scientific). Two 6-points, matrix-matched multi-element standard curves with concentrations bracketing the range of the samples were run at the beginning, the middle and the end of each analytical run. Analytical replicates were made every 10 samples, while accuracy was determined by performing digestions of the certified reference material BCR-414 (plankton, Community Bureau of Reference, Commission of the European Communities), PACS-3 and MESS-4 (marine sediments, National Research Council Canada), following the same protocol as for samples. Recoveries were typically within 10% of the certified values (and within the error of the data, taken from replicate measurements, Table 1). Once all data

were normalized to an ^{115}In internal standard and quantified using an external standard curve, the dilution factor of the total digestion was accounted for. Obtained element concentrations per filter (pmol/filter) were then corrected by the process blanks described above. Finally, pmol/filter values were divided by the volume of water filtered through stacked filters.

Total concentrations (sum of small size fraction (0.45-5 µm) and large (>5 µm) size fraction) of particulate trace elements are reported in Table S1 (supplementary data).

2.4. Ancillary data:

Potential temperature (θ), salinity (S), and transmissometry data were retrieved from the CTD sensors (CTD SBE911 equipped with a SBE43).

2.5. Positive matrix factorisation

Positive Matrix Factorisation (PMF) was run to characterise the main factors influencing the particulate trace elements variances along the GEOVIDE section. In addition to PFe, PAl, PMn, and PP, nine additionnal elements were included in the PMF: Y, Ba, Pb, Th, Ti, V, Co, Cu and Zn. The analysis has been conducted on samples where all the 13 elements previously cited were above the detection limits; after selection, 445 of the 549 existing data points were used. Analyses were performed using the PMF software, EPA PMF 5.0, developed by the USA Environmental Protection Agency (EPA). Models have been tested with several factors number (from 3 to 6), after full error estimation of each model, we decide to use the configuration providing the lowest errors estimations and in consequence the most reliable.

In consequence, models were set up with four factors and were run 100 times to observe the stability of the obtained results. After displacement, error estimations and bootstraps error estimations, the model was recognised as stable.

3. Results

3.1. Hydrography and biological setting

Here, we briefly describe the hydrography encountered during the GEOVIDE section (Figure 2), as a thorough description is available in García-Ibáñez et al. (2015). The warm and salty Mediterranean Water (MW, S=36.50, θ°=11.7°C) was sampled between 600 and 1700 m in the Iberian Abyssal Plain (IAP). MW resulted from the mixing between the Mediterranean Overflow Water plume coming from the Mediterranean Sea and local waters. Surface water above the Iberian Shelf was characterised by low salinity (S=34.95) at station 2 and 4 compared to surrounding water masses. Close to the floor of the Iberian Abyssal Basin, the North East Atlantic Deep Water (NEADW, S=34.89, θ°=2.0°C) spread southward. The North Atlantic Central Water (NACW, S>35.60, θ°>12.3°C) was the warmest water mass of the transect and was observed in the subsurface layer of the Western European Basin and Iberian Abyssal Plain. An old Labrador Sea Water (LSW, S=34.87, θ°=3. 0°C) flowed inside the Western European and Icelandic Basins, between 1000 and 2500m depth. In the Icelandic Basin, below the old LSW, the Iceland-Scotland Overflow Water (ISOW, S=34.98, θ°=2.6°C) spread along the Reykjanes Ridge slope. This cold water, originating from the Arctic, led to the formation of NEADW after

mixing with surrounding waters. North Atlantic hydrography was impacted by the northward flowing of the North Atlantic Current (NAC), which carried up warm and salty waters from the subtropical area. When NAC crossed the Mid-Atlantic ridge through the Charlie-Gibbs Fracture Zone (CGFZ), it created the Subpolar Mode Water (SPMW). The recirculation of SPMW inside the Icelandic and Irminger Basins led to the formation of regional modal waters: the Iceland Subpolar Mode Water (IcSPMW, S=35.2, θ°=8.0°C) and the Irminger Subpolar Mode Water (IrSPMW, S=35.01, θ°=5.0°C) respectively. IcSPMW was a relatively warm water mass with potential temperature up to 7°C (García-Ibáñez et al., 2015). Another branch of the NAC mixed with Labrador Current waters to form the relatively fresh SubArctic Intermediate Water (SAIW, S=<34.8, 4.5°C<θ°<6°C). The Irminger Basin is acomplex area with a multitude of water masses. In the middle of the basin, an old LSW, formed one year before (Straneo et al., 2003), spread between 500 and 1200 m depth. Close to the bottom, the Denmark Strait Overflow Water (DSOW, S=34.91) flowed across the basin. Greenland coastal waters were characterised by low salinity values, down to S=33. The strong East Greenland Current (EGC) flowed southward along the Greenland shelf in the Irminger Basin. When reaching the southern tip of Greenland, this current entered the Labrador Basin along the west coast of Greenland and followed the outskirts of the basin until the Newfoundland shelf. In the Labrador Basin, the deep convection of SPMW at 2000 m was involved in the formation of the LSW (S=34.9, θ°C=3.0°C) (García-Ibáñez et al., 2015; Yashayaev and Loder, 2009). Above the Newfoundland Shelf, surface waters were affected by discharge from rivers and ice-melting and characterised by extreme low salinity for open ocean waters, below 32 in the first 15 meters.

3.2. Section overview

Total particulate iron (PFe), aluminium (PAl), manganese (PMn) and phosphorus (PP) concentrations spanned a large range of concentrations from below detection to 304, 1544, 3.5 and 402 nmol L^{-1} respectively.
PFe, PAl, and PMn were predominantly found (>90%) in particles larger than 5 µm, except in surface waters, where 9 ± 8.6 % of PFe, 38.8 ± 8.6 % of PP, 10.9 ± 15.4 % of PAl and 32.8 ± 16.6 % of PMn were hosted by smaller particles (0.45-5 µm). The ranges of concentrations are comparable to other studies recently published (Table 2). Data are shown in Figure 3.

3.3. Open Ocean stations :Iberian Abyssal Plain (stations 11 to 17), Western European Basin (stations 19 to 29), Icelandic Basin (stations 32 to 36), Reykjanes Ridge (station 38), Irminger Basin (stations 40 to 60; except Stations 53 and 56) and Labrador Basin (stations 63 to 77)

Particulate iron concentration vertical profiles presented identical patterns at open ocean stations sampled in each oceanic basin encountered along the section. Median PFe were low at 0.25 nmol L^{-1} within the first 100 m and steadily increased with depth. However, at two stations, elevated concentrations were determined in the upper 100m, up to 4.4 nmol L^{-1} at station 77 at 40 m and 7 nmol L^{-1} at station 63 between 70 and 100 m depth. PFe concentrations gradually increased with depth, with a median PFe of 1.74 nmol L^{-1} below 1000m. Close to the seafloor of some stations (26, 29, 32, 34, 49, 60, and 71), high concentrations of PFe were observed, up to 88 nmol L^{-1} (station 71 at 3736 m). These high PFe values were associated with low beam transmissometry value inferior or equal to 97 % (Figure 9b and supplementary table S2).

Particulate aluminium (PAl) and manganese (PMn) profiles were similar to PFe profiles, with low concentrations measured in the first 100 m (1.88 nmol L^{-1} and 55 pmol L^{-1}, respectively) and increased towards the seafloor. Close to the seafloor, high concentrations were determined at the same stations cited above for PFe, with a maximum of 264 nmol L^{-1} and 3.5 nmol L^{-1} for PAl and PMn respectively at station 71 (supplementary Table S1). Highest particulate phosphorus (PP) concentrations were in the first 50m, with a median value of 66 nmol L^{-1}. Deeper in the water column, below 200m, PP concentrations decreased to values below 10 nmol L^{-1}. Inter-basins differences were observed within the surface samples, with median PP concentration being higher in the Irminger Basin (127 nmol L^{-1}) than in the Iberian Abyssal Plain (28 nmol L^{-1}).

Finally, above the Reykjanes Ridge, PP, PMn, PAl and PFe concentrations were in the same range than the surrounding open ocean stations. However, close to the seafloor, high concentrations were measured, with PFe, PAl, and PMn reaching 16.2 nmol L^{-1}, 28.8 nmol L^{-1}, and 0.51 nmol L^{-1} at 1354 m, respectively (Figure 3 and supplementary material Table S1).

3.4. Margins and Shelves: Iberian Margin (stations 1 to 4), Greenland coast (stations 53, 56 and 61) and Newfoundland Shelf (station78)

The Iberian margin was characterised by low beam transmissometry values at station 2 (88% at 140 m, Figure 9b) suggesting significant particle concentrations. Particulate iron concentrations varied between 0.02 nmol L^{-1} to 304 nmol L^{-1}. Within the first 50m, PFe concentrations decreased towards the shelf break where PFe dropped down from 2.53 nmol L^{-1} (station 2) to 0.8 nmol L^{-1} (Station 1). PFe concentrations increased with depth at all three stations and reached a maximum at the bottom of station 2 (138.5 m) with more than 300 nmol L^{-1} of PFe. Lithogenic tracers, such as PAl or PMn, presented similar profiles to PFe with concentrations ranging between 0.11 and 1544 nmol L^{-1}, and from below detection limit to 2.51 nmol L^{-1} respectively (Figure 3, supplementary material Table S1). Total particulate phosphorus (PP) concentrations were relatively low in surface ranging from undetectable values to 38 nmol L^{-1}; concentrations decreased with depth and were less than 0.7 nmol L^{-1} below 1000 m depth.

In the vicinity of the Greenland shelf, PFe concentrations had a high median value of 10.8 nmol L^{-1} and were associated with high median PAl and PMn concentrations of 32.3 nmol L^{-1} and 0.44 nmol L^{-1}, respectively. Concentrations of PP were high at the surface with a value of 197 nmol L^{-1} at 25 m of station 61. Then, PP concentrations decreased strongly, less than 30 nmol L^{-1}, below 100 meters depth. Furthermore, beam transmissometry values in surface waters at these three stations, were the lowest of the entire section, with values below 85 %.

Close to the Newfoundland margin, surface waters displayed a small load of particulate trace metals as PFe, PAl, and PMn were below 0.8 nmol L^{-1}, 2 nmol L^{-1}, and 0.15 nmol L^{-1} respectively. Then close to the bottom of station 78, at 371 m, beam transmissometrytry values dropped to 94% and were associated with extremely high concentrations of PFe=168 nmol L^{-1}, PAl=559 nmol L^{-1}, and PMn=2 nmol L^{-1}. Total PP concentrations in the first 50 m ranged from 35 to 97 nmol L^{-1}. Below the surface, PP remained relatively high with values up to 16 nmol L^{-1} throughout the water column. (Figure 3 and supplementary material Table S1).

4. Discussion

Our goal in this work was to investigate mechanisms that drive the distribution of PFe in the North Atlantic, in particular the different routes of supply and removal. Possible candidate sources of PFe include lateral advection offshore from margins, atmospheric inputs, continental run-off, melting ice shelves and icebergs, resuspended sediments, hydrothermal inputs and biological uptake. Removal processes include remineralization and dissolution processes.

In the following sections, we examine each of these sources and processes, explore the evidence for their relative importance, and use compositional data to estimate the particle types and host phases for iron and associated elements.

4.1. Analysis of the principal factors controlling variance: near-ubiquitous influence of crustal particles in the water column

The positive matrix factorisation results, shown in Figure 5, indicate the overall variances explained by each of the 5 factors. The first factor is characterised by lithogenic elements, representing 86.8% of the variance of PFe, 75.8% of PAl and 90.5% of PTi. The second factor is correlated with both Mn and Pb and explains no less than 76.5% and 77.0% of their respective variances. Ohnemus and Lam (2015) observed this co-relation between manganese and lead particles and explained it by the co-transport on Mn-oxides (Boyle et al., 2005). The formation of barite is causing the third factor constraining 87.7% of the Ba variance in the studied regions. Biogenic barite accumulation within the mesopelagic layer is related to bacterial activity and organic remineralisation (Lemaitre et al., 2018a). A biogenic component is the fourth factor and explained most of particulate phosphorus variance, 83.7%. The micronutrient trace metals, copper, cobalt and zinc, had more than a quarter of their variances influenced by this factor.

These results indicate that along the GA01 section, PFe distributions were predominantly controlled by lithogenic material and to a smaller extent by remineralisation processes (as seen by a Factor 3 contribution of 4.1%). This does not rule out some biogenic influence on PFe distribution, especially in surface, but this contribution is veiled by the high lithogenic contribution. The PMF analysis has been realised on the entire dataset, in consequence, the factors described are highly influenced by the major variations of particulate element concentrations (usually at the interface, i.e. margin, seafloor, surface layer,...).

To further investigate the influence of crustal material on the distribution of PFe, it is instructive to examine the distribution of the molar ratio of PFe/PAl along the section as a way to assess the lithogenic inputs (Lannuzel et al., 2014; Ohnemus and Lam, 2015; Planquette et al., 2009) (Figure 6) along the section.

The PFe/PAl ratio can be used to estimate the proportion of lithogenic particles within the bulk particulate material. A comparison with the Upper Continental Crust (UCC) ratio of Taylor and McLennan (1995), 0.21, was used to calculate the lithogenic components of particles (PFe_{litho}) following Eq. (1):

$$\%\text{PFe litho} = 100 * \left(\frac{\text{PAl}}{\text{PFe}}\right)\text{sample} * \left(\frac{\text{PFe}}{\text{PAl}}\right)\text{UCC ratio} \qquad (1)$$

Then the non-lithogenic PFe is simply obtained using Eq. (2):

$$\%\text{PFe non\_litho} = 100 - \%\text{PFe litho} \qquad (2)$$

Both the lithogenic and non-lithogenic fraction of PFe are estimated using the UCC ratio. Spatial and temporal variation of the lithogenic components ratio may falsely influence the estimated fraction value. The PFe_{litho} and $PFe_{non\text{-}litho}$ proxies are interesting tools to evaluate the importance of lithogenic and non-lithogenic (either biogenic or authigenic), but have to be used with consideration.

Overall, the estimated lithogenic contribution to PFe varies from 25% (station 60, 950 m) to 100% at stations located within the Western European Basin. 100% of estimated lithogenic PFe doesn't necessary mean that biogenic particles are absent; they may just be masked by the important load of lithogenic particles. Important inter-basins variations are observed along the section (Figure 6). The IAP and WEB basins are linked with high median value of the proxy $\%Fe_{litho}$, 90%. This could be linked to a lateral advection of iron rich lithogenic particles sourced from the Iberian margin and to atmospheric particles (Shelley et al., 2017). This point is discussed with more detail in section 4.3.1. While the Iceland, Irminger and the Labrador basins are characterised with median %PFe value under 55%. An interesting feature observable was the dramatic decrease of the %PFe proxy values happening at the station 26 (Figure 6). This feature is likely be associated to the presence of the Sub-Arctic Front, located between 49.5 and 51°N latitude and 23.5 and 22°W longitude (Zunino et al., 2017). Indeed, this front which separates cold and fresh water of subpolar origin from warm and salty water of subtropical origin was clearly identifiable at station 26 by the steep gradient of the isotherms and isohalines (Figure 2).

4.2. Fingerpriting watermasses

The GEOVIDE section crossed several distinct water masses along the North Atlantic, each of them being distinguishable by their salinity and potential temperature signatures (García-Ibáñez et al., 2015; Figure 2). Based on this study, we applied a Kruskal-Wallis test on molar PFe/PAl ratios of nine water masses (Figure 7) in order to test the presence of significant differences. Water masses for which we had less than 5 data points for PFe/PAl were excluded from this test. As the differences in the median values among the treatment groups were greater than would be expected by chance; the difference in PFe/PAl between water masses is statistically significant ($P = <0.001$).

As previously seen, the lithogenic inprint is dominant in the WEB, with MW and NEADW showing PFe/PAl values close to the UCC value of 0.21 mol mol^{-1}. Interestingly, the PFe/PAl signature of 0.36 mol mol^{-1} within the old LSW_{WEB} is probably due to the effect of biologic inputs associated with the strong bloom encountered in the Irminger Sea than in the WEB (see section 4.3.5). While it appears that lithogenic particles are dominating the water column in the WEB and that some water masses have a clear PFe/PAl fingerprint, it is important to discuss the origin of these signatures, which is the purpose of the following sections.

4.3. Tracking the different inputs of particulate iron

4.3.1. Inputs at margins: Iberian, Greenland and Newfoundland

Inputs from continental shelves and margins have been demonstrated to support high productivity in shallow coastal areas. Inputs of iron from continental margin sediments supporting the high productivity found in shallow coastal regions have been demonstrated in the past (e.g. Cullen et al. (2009), Elrod et al. (2004), Jeandel et al. (2011), Ussher et al. (2007)) and sometimes, were shown to be advected at great distances from the coast (e.g. Lam et al., 2008).

In the following section, we will investigate these possible candidate sources in proximity of the different margins encountered. Along the GEOVIDE section, sediments at margins were of various compositions (Dutkiewicz et al., 2015). Sediments originating from the Iberian margin were mainly constituted of silts and clays (Cacador et al., 1996; Duarte et al., 2014). East Greenland margin sediments were a mixture of sands and grey/green muds, while, sediments from the West Greenland margin were mainly composed of grey/green muds (Loring and Asmund, 1996). At the western end of the section, sediments from the Newfoundland margin were composed of gravelly and sandy muds (Mudie et al., 1984). The different sediment compositions of the three margins sampled during GEOVIDE have different mineralogy/composition, which are reflected in their different PFe/PAl ratios (Figure 8). While the Iberian Margin had a PFe/PAl close to UCC ratio, the highest ratio could be seen at the East Greenland (stations 53 and 56) and West Greenland (station 61) Margins, with median PFe/PAl reaching 0.45 mol mol-^{1}. The Newfoundland margin displayed an intermediate behaviour, with Fe/Al ratios of 0.35 mol mol^{-1}.

In addition to PAl, PMn can be used as a tracer of inputs from shelf resuspension (Lam and Bishop, 2008). Indeed, Mn is really sensitive to oxidation mediated by bacteria (Tebo et al., 1984; Tebo and Emerson, 1985) and forms manganese oxides (MnO_2). These authigenic particles lead to an enrichment of Mn in particle compositions. In order to track the influence of shelf resuspension, a percentage of sedimentary inputs "%bulk sediment inputs" can be estimated using PMn/PAl ratio from GEOVIDE samples and the PMn/PAl UCC value (0.0034; Taylor and McLennan, 1995) according to the following equation:

$$\%\text{bulk sediment PMn} = 100 * \left(\frac{\text{PAl}}{\text{PMn}}\right)\text{sample} * \left(\frac{\text{PMn}}{\text{PAl}}\right)\text{UCC ratio} \quad (3)$$

This proxy is a good indicator of direct and recent sediment resuspension. We assume that particles newly resuspended in water column will have the same PMn/PAl ratio than the UCC ratio leading to a "%bulk sediment Mn" of 100%. This value will decrease by authigenic formation of Mn oxides. This proxy assumes homogeneity of the sediment PMn/PAl ratio through the section which is maybe not completely the case at every station. In consequence, this proxy is only a tool to identify new benthic resuspension at specific location and inter-comparison between several locations is not possible. When a sample presents a "%bulk sediment Mn" greater than 100%, we assign a value of 100% to simplify the following discussion. As the Mn cycle can also be affected by biologic uptake (e.g. Peers and Price, 2004; Sunda and Huntsman, 1983), this proxy is only used at depths where biologic activity is negligible (i.e. below 150m depth).

The Iberian margin

Coastal waters of the Iberian Shelf are impacted by the runoff for the Tagus River, which is characterised by high suspended matter discharges, ranging between 0.4 to 1 × 10^{6} tons yr^{-1}, and with a high anthropogenic signature (Jouanneau et al., 1998). During the GEOVIDE section, the freshwater input was observable at

stations 1, 2 and 4 in the first 20 m; salinity was below 35.2 psu while surrounding waters masses had salinity up to 35.7 psu. Within the freshwater plume, particulate concentrations were important at station 2 with PFe of 1.83 nmol L^{-1}. Further away from the coast, the particulate concentrations remained low at 20m depth, with PFe, PAl, and PMn concentrations of 0.77 nmol L^{-1}, 3.5 nmol L^{-1}, and 0.04 nmol L^{-1}, respectively at station 1. The low expansion of the Tagus plume is likely due to the rapid settling of suspended matter. Indeed, our coastal station 2 was already located at around 50 km of the Iberian coast and according to Jouanneau et al. (1998), the surface particle load can be observable at a maximum 30km of the Tagus estuary.

Besides, ADCP data acquired during GEOVIDE (Zunino et al., 2017) and several studies have reported an intense current spreading northward coming from Strait of Gibraltar and Mediterranean Sea, leading to a strong resuspension of benthic sediments above the Iberian Shelf, e.g. Biscaye and Eittreim (1977), Eittreim et al. (1976), McCave and Hall (2002), Spinrad et al. (1983). The importance of the sediment resuspension was observable by low beam transmissometry value (87.6%) at the bottom of station 2. This important sediment resuspension led to an extensive input of lithogenic particles within the water column associated with high concentrations of PFe (304 nmol L^{-1}), PAl (1500 nmol L^{-1}), and PMn (2.5 nmol L^{-1}) (Figure 3, Table S1). Moreover, one hundred percent of PFe is estimated to have a lithogenic origin (Figure 10) while 100% of the PMn was estimated to be the result of a recent sediment resuspension according to the $\%Fe_{litho}$ and "%bulk sediment Mn" proxies (supplementary material, Table S2), confirming the resuspended particle input.

At distance from the shelf, within the Iberian Abyssal Plain, an important lateral advection of PFe from the margin was observable (Figure 10). These lateral inputs occurred at two depth ranges: between 400 and 1000 m as seen at stations 4 and 1, with PFe concentrations reaching 4 nmol L^{-1}, and between 2500 m and the bottom (3575 m) of station 1, with PFe concentrations reaching 3.5 nmol L^{-1}. While 100% of PFe had a lithogenic signature, the sedimentary source input estimation decreased, between 40% and 90% of the PMn (Figure 10). Transport of lithogenic particles was observable until station 11 (12.2°W) at 2500 m where PFe concentration was 7.74 nmol L^{-1} and 60% of PMn had a sedimentary origin (Figure 9). Noteworthy, no particular increase in PFe, PMn or PAl was seen between 500 and 2000 m depth, where the MOW spreads, which is consistent with that was observed DFe concentrations (Tonnard et al., this issue); yet in contrast with the dissolved aluminium values (Menzel Barraqueta et al, subm., this issue) which were high in the MOW and with the study of Ohnemus and Lam (2015) that reported a maximum PFe concentration at 695 m depth associated with the particle-rich Mediterranean Overflow Water (Eittreim et al., 1976) in the IAP. However, their station was located further south of our station 1. The shallower inputs observed at stations 1 and 4 could therefore be attributed to sediment resuspension from the Iberian margin and nepheloid layer at depth for station 1.

Therefore, the Iberian margin appears to be an important source of lithogenic-derived iron-rich particles in the Atlantic Ocean; shelf resuspension impact was perceptible until 280 km away from the margin (Station 11) in the Iberian Abyssal Plain.

South Greenland

Several studies already demonstrated the importance of icebergs and sea ice as source of dissolved and particulate iron (e.g. van der Merwe et al., 2011a, 2011b; Planquette et al., 2011; Raiswell et al., 2008). The Greenland shelf is highly affected by external fresh water inputs as ice-melting or riverine runoff (Fragoso et al.,

2016), that are important sources of iron to the Greenland Shelf (Bhatia et al., 2013; Hawkings et al., 2014; Statham et al., 2008).

Both East and West Greenland shelves (stations 53 and 60) had high concentration of particles (beam transmissometry of 83%) and particulate trace elements, reaching 22.1 nmol L^{-1} and 18.7 nmol L^{-1} of PFe, respectively (station 53 at 100m and station 61 at 136 m). During the cruise, the relative freshwater observed (S<33 psu) within the first 25 meters of stations 53 and 61 were associated with high PFe (19 nmol L^{-1}), PAl (61 nmol L^{-1}), PMn (0.6 nmol L^{-1}) and a low beam transmissometry (≤ 85%) (Figure 9 and Table S1). Particles associated were enriched in iron compared to aluminium, as PFe/PAl ratio was 0.3 within the meteoric water plume. High biological production, in agreement with PP concentrations reaching 197 nmol L^{-1} induced by the supply of bioavailable dissolved iron from meteoric water (Raiswell et al., 2008; Statham et al., 2008;, Tonnard et al., submitted, this issue), led to a transfer of DFe to the particulate phase. This is in line with the fact that around 30% PFe had a non-lithogenic origin. In addition, only 40% PMn originated from resuspended sediments. Interestingly, these two proxies remained constant from the seafloor to the surface (Station 49, Figure 10), with around 25% of the PMn of sedimentary origin, which could be due to an important mixing happening on the shelf. The lithogenic PFe could result from the release of PFe from Greenland bedrock captured during the ice sheet formation on land. The spatial extent of the off-shelf lateral transport of particles was not important on the east Greenland coast. Indeed, no visible increase of particulate trace metal concentrations was visible at the first station off-shelf, station 60 (Figure 10), except at 1000 m depth, where a strong increase (up to 90%) of sedimentary PMn was seen. This is probably due to the East Greenland Coastal Current (EGCC) that was located at station 53 constrained these inputs while stations 56 and 60 were under the influence of another strong current, the East Greenland-Irminger current (EGIC) (Zunino et al., 2017).

To the west of the Greenland margin, lateral transport of particles was slightly more important. Noticeable concentrations of particulate lithogenic elements were observable until station 64 located 125 km away from shoreline. These particles had decreasing PFe lithogenic contribution (50%) with a similar (25%) sedimentary PMn content than closer to the margin. The increasing nature of non-lithogenic PFe is linked to the bloom in surface (associated with a PFe/PAl ratio of 0.30 mol mol^{-1}, a PP of 197 nmol L^{-1} at station 61 and a Chl-a concentrations of 6.21 mg m^{-3}), with the biogenic PFe settling down along the transport of particles.

Therefore, particles newly resuspended from Greenland sediments are an important source, representing around a third of the pMn pool, combined with surface inputs such as riverine runoff and/or ice-melting that are delivering particles on the shelf and biological production. Unlike the Iberian shelf, Greenland margin was not an important provider of particulate metals inside the Irminger and Labrador Basin, due to the circulation that constrained the extent of the margin plume.

The Newfoundland Shelf

Previous studies already described the influence of fresh water on the Newfoundland shelf from the Hudson Strait and/or Canadian Artic Archipelago (Fragoso et al., 2016; Yashayaev, 2007). Yashayaev (2007) also monitored strong resuspension of sediments associated with the spreading of Labrador Current along the West Labrador margin.

Close to the Newfoundland coastline, at station 78, high fresh water discharge (≤ 32 psu) was observed in surface (Benetti et al., 2017). Interestingly, these freshwater signatures were not associated with elevated

particulate trace metal concentrations. Distance of meteoric water sources implied a long travel time for the water to spread through the Labrador Basin to our sampling stations. Along the journey, particles present originally may have been removed from water column by gravitational settling.

The proportion of lithogenic PFe was relatively high and constant in the entire water column, with a median value of 70%. At station 78, 100% of the PMn had a sedimentary origin close to the seafloor (371 m). The spreading of the recent sediment resuspension was observable until 140 m depth where the contribution of sedimentary Mn was still 51% (Figure 10, Table S2). This could correspond to an intense nepheloid layer as previously reported by Biscaye and Eittreim (1977) (see also section 3.3.2). The high PFe concentration (184 nmol L^{-1}, station 78, 371 m) associated with a high percentage of sedimentary PMn (95%) observed at the bottom of this station, was therefore the result of an important resuspension of shelf sediments. This was confirmed with low transmissometry values of 95%.

The important phytoplanktonic community present (maximum Chl-a= 4.91 mg m^{-3}, Tonnard et al., in prep), is linked to low PFe of 0.79 nmol L^{-1} at 10 m, but, with a high PFe/PAl ratio, up to 0.4, and PP concentration of 97 nmol L^{-1}, confirming the biologic influence. Either the biogenic particles settled quickly, and/or they were quickly remineralized. Concerning this latter process, intense remineralization at station 77 (7 mmol C m^{-2} d^{-1} compared to 4 mmol C m^{-2} d^{-1} in the Western European Basin) has been reported by Lemaitre et al. (2018a and 2018b), which could explain the low PFe values throughout the water column.

Along the GEOVIDE section, continental shelves provided an important load of particles within the surrounding water column. The three margins sampled during GEOVIDE behaved differently; the Iberian margin discharged high quantities of lithogenic particles far away from the coast while the Greenland and Newfoundland margins did not reveal important PFe concentrations. Spreading of particles is tightly linked to hydrodynamic conditions, which in the case of the Greenland margin, prevented long distance seeding of PFe. Moreover, each margin showed a specific PFe/PAl ratio (Figure 8) indicating different composition of the resuspended particles. Resuspended particles represent the composition of sediment at the margin if oxido-reductive transformation of iron and aluminium are considered negligible under these circumstances. Differences between margins were due to the presence of non-crustal particles, either biogenic or authigenic. Biological production in surface waters and authigenic formation of iron hydroxide produce particles with a higher PFe/PAl content and their export through the water column to the sediment increased the PFe/PAl ratio at depth. Regions where biological production is intense such as in the vicinity of Newfoundland presented higher PFe/PAl ratios of resuspended benthic particles.

4.3.2 Benthic resuspended sediments

Benthic nepheloid layers (BNLs) are important layers where local resuspension of sedimentary particles (Bishop and Biscaye, 1982; Eittreim et al., 1976; Rutgers Van Der Loeff et al., 2002) occur due to strong hydrographic stresses (i.e. boundary currents, benthic storms and deep eddies) interacting with the ocean floor (Biscaye and Eittreim, 1977; Eittreim et al., 1976; Gardner et al., 2017, 2018). Along the GA01 section, BNLs were observable in each province with different strengths (Figures 3 and 12).

In BNLs located within the WEB, PFe concentrations reached up to 10 nmol L^{-1} (stations 26 and 29, Table S1). These concentrations were smaller than PFe concentrations encountered in BNL from the Icelandic, Irminger

and Labrador Basins, where benthic resuspension led to PFe concentrations higher than 40 nmol L^{-1}, even reaching 89 nmol L^{-1} at the bottom of station 71 (3736 m). Moreover, in the Irminger and Labrador Basins, PFe/PAl molar ratios within BNLs were higher than the ones measured within the WEB at station 26 and 29. In the Irminger Basin, PFe/PAl reached 0.4 mol mol^{-1}, which could reveal a mixture of lithogenic and biogenic matter previously exported. This feature was also observed in the Labrador Basin, with PFe/PAl ratio ranging between 0.34 and 0.44 mol mol^{-1}. In contrast, BNLs sampled in the WEB have clearly a lithogenic imprint, with PFe/PAl molar ratios close to the crustal one. Resuspended sediments with a non-crustal contribution seem to hold a higher PFe content than sediments with a lithogenic characteristic. Nevertheless, interestingly all BNLs present during GEOVIDE were spreading identically, with impacts observable up to 200 meters above the oceanic seafloor (Figure 11), as reflected in beam transmissometry values, and PFe concentrations, that returned to a background level at 200 m above the seafloor. The presence of these BNLs has also been reported by Le Roy et al. (submitted, this issue). Important differences of PFe intensities could also be due to different hydrographic components and topographic characteristics. As previously explained, two main triggers of BNLs are benthic storms and deep eddies; by definition these processes are highly variable geographically and temporally, but no physical data could allow us to investigate further this hypothesis.

Along the GEOVIDE section, BNLs are providing high concentrations of particulate trace element in the deep open ocean, contributing highly to the total trace elements budget as iron.

4.3.3. Reykjanes Ridge inputs

Above the ridge, high PFe concentrations were measured, reaching 16 nmol L^{-1} just above the seafloor, while increased DFe concentrations were reported to the East of the ridge (Tonnard et al., this issue). The exact sources of iron-rich particles cannot be well constrained, as they could come from active hydrothermal vents or resuspension of particulate matter from new crustal matter produced at the ridge. According to the oceanic circulation (Zunino et al., 2017; Garcia-Ibanez et al., 2017), hydrothermal particles could have been seen in the ISOW within the Icelandic Basin. Nevertheless, at the vicinity of the ridge, scanning electron microscope (SEM) analyses of our samples did reveal a number of biological debris and clays but not the presence of iron (oxy-)hydroxide particles, which are known to be highly produced close to hydrothermal vents (Elderfield and Schultz, 1996). Their absence could thus indicate an absence of vents. However, other proxies, such as helium-3, are necessary to claim with more accuracy the presence or absence of an hydrothermal source close to station 38.

4.3.4. Atmospheric inputs

Atmospheric deposition is an important input of trace elements in surface of the open ocean (e.g. (Jickells et al., 2005). Atmospheric inputs, both wet and dry, were reported to be low during the GEOVIDE cruise (Menzel-barraqueta et al., 2018, this issue; Shelley et al., 2017; 2018). In fact, oceanic particles measurements in surface waters along the section did not reveal high PFe or PAl concentrations, therefore, the surface composition of particles did not seem to be highly affected by atmospheric deposition at the time of the cruise. One pattern is also interesting to note: the surface waters of the Iberian Abyssal Plain and Western European Basin, between stations 11 and 23 presented a characteristic feature with really low PFe/PAl elemental ratios, of 0.11, smaller

than the UCC ratio of 0.21 (Figure 6). Such low ratios have been reported in the same region by Barrett et al. (2012). One possible explanation is given by Buck et al. (2010) who described Fe-depleted aerosols in this area of the North Atlantic with PFe/PAl ratio below UCC ratio. However, Shelley et al. (2017) found a higher PFe/PAl ratio around 0.25 is this area (their sample geoa5-6). This result, highlights some of the difficulties that link atmospheric inputs to water column data (Baker et al., 2016), and implies a probable fractionation after aerosol deposition. In addition, there is high spatial and temporal variability of atmospheric deposition (Mahowald et al., 2005) and a certain degree of uncertainty about the dissolution processes of atmospherically-transported particles (Bonnet and Guieu, 2004).

5. Conclusions

This investigation of the PFe compositions of suspended particulate matter in the North Atlantic indicates the pervasive influence of crustal particles, augmented by sedimentary inputs at margins, and at depths, within benthic nepehloid layers.

Indeed, along the GEOVIDE section, continental shelves provided an important load of particles within the surrounding water column, with PFe mostly residing in non-biogenic particulate form. The Iberian margin discharged high quantities of lithogenic particles originating from riverine inputs far away from the coast while the Greenland margin did not reveal a long distance seeding of PFe, due to hydrodynamic conditions. Both Greenland and Newfoundland margins PFe resuspended particles were under a strong biogenic influence that were exported at depth. This resulted in different remineralisation fluxes among the different provinces. Scavenging processes could also be visible at depths greater than 1000 m, these effects being the most pronounced within the Labrador Basin.

Finally, resuspended sediments above the Reykjanes Ridge increased the PFe composition of the Iceland Scottish Overflow Water. A similar feature occurs for the Labrador Sea Water, as it flows from the Irminger Basin to the Western European Basin.

Acknowledgments

We are greatly indebted to the captain and crew of the N/O Pourquoi Pas? for their help during the GEOVIDE mission and clean rosette deployment. We would like to give special thanks to Fabien Pérault and Emmanuel de Saint Léger for their technical expertise, to Catherine Schmechtig for the GEOVIDE database management and Greg Cutter for his guidance in setting up the new French clean sampling system. We also would like to thanks Reiner Schlitzer for the Ocean Data View software (ODV).

This work was supported by the French National Research Agency (ANR-13-BS06-0014, ANR-12-PDOC-0025-01), the French National Centre for Scientific Research (CNRS-LEFE-CYBER), the LabexMER (ANR-10-LABX-19), and Ifremer. It was supported for the logistic by DT-INSU and GENAVIR.

References

Aguilar-Islas, A. M., Rember, R., Nishino, S., Kikuchi, T. and Itoh, M.: Partitioning and lateral transport of iron to the Canada Basin, Polar Sci., 7(2), 82–99, doi:10.1016/j.polar.2012.11.001, 2013.

Baker, A. R., Adams, C., Bell, T. G., Jickells, T. D. and Ganzeveld, L.: Estimation of atmospheric nutrient inputs to the Atlantic Ocean from 50°N to 50°S based on large-scale field sampling: Iron and other dust-associated elements, Global Biogeochem. Cycles, 27(3), 755–767, doi:10.1002/gbc.20062, 2013.

Baker, A. R., Landing, W. M., Bucciarelli, E., Cheize, M., Fietz, S., Hayes, C. T., Kadko, D., Morton, P. L., Rogan, N., Sarthou, G., Shelley, R. U., Shi, Z., Shiller, A. and van Hulten, M. M. P.: Trace element and isotope deposition across the air–sea interface: progress and research needs, Philos. Trans. R. Soc. A Math. Phys. Eng. Sci., 374(2081), 20160190, doi:10.1098/rsta.2016.0190, 2016.

Barrett, P. M., Resing, J. A., Buck, N. J., Buck, C. S., Landing, W. M. and Measures, C. I.: The trace element composition of suspended particulate matter in the upper 1000m of the eastern North Atlantic Ocean: A16N, Mar. Chem., 142–144, 41–53, doi:10.1016/j.marchem.2012.07.006, 2012.

Berger, C. J. M., Lippiatt, S. M., Lawrence, M. G. and Bruland, K. W.: Application of a chemical leach technique for estimating labile particulate aluminum, iron, and manganese in the Columbia River plume and coastal waters off Oregon and Washington, J. Geophys. Res., 113, C00B01, doi:10.1029/2007JC004703, 2008.

Bergquist, B. A., Wu, J. and Boyle, E. A.: Variability in oceanic dissolved iron is dominated by the colloidal fraction, Geochim. Cosmochim. Acta, 71(12), 2960–2974, doi:10.1016/j.gca.2007.03.013, 2007.

Bhatia, M. P., Kujawinski, E. B., Das, S. B., Breier, C. F., Henderson, P. B. and Charette, M. A.: Greenland meltwater as a significant and potentially bioavailable source of iron to the ocean, Nat. Geosci., 6(4), 274–278, doi:10.1038/ngeo1746, 2013.

Biscaye, P. E. and Eittreim, S. L.: Suspended Particulate Loads and Transports in the Nepheloid Layer of the Abyssal Atlantic Ocean, Dev. Sedimentol., 23(C), 155–172, doi:10.1016/S0070-4571(08)70556-9, 1977.

Bishop, J. K. B. and Biscaye, P. E.: Chemical characterization of individual particles from the nepheloid layer in the Atlantic Ocean, Earth Planet. Sci. Lett., 58(2), 265–275, doi:10.1016/0012-821X(82)90199-6, 1982.

Bishop, J. K. B. and Fleisher, M. Q.: Particulate manganese dynamics in Gulf Stream warm-core rings and surrounding waters of the N.W. Atlantic, Geochim. Cosmochim. Acta, 51(10), 2807–2825, doi:10.1016/0016-7037(87)90160-8, 1987.

Bonnet, S.: Dissolution of atmospheric iron in seawater, Geophys. Res. Lett., 31(3), L03303, doi:10.1029/2003GL018423, 2004.

Boyle, E. A., Bergquist, B. A., Kayser, R. A. and Mahowald, N.: Iron, manganese, and lead at Hawaii Ocean Time-series station ALOHA: Temporal variability and an intermediate water hydrothermal plume, Geochim. Cosmochim. Acta, 69(4), 933–952, doi:10.1016/j.gca.2004.07.034, 2005.

611 Buck, C. S., Landing, W. M., Resing, J. A. and Measures, C. I.: The solubility and deposition of aerosol Fe and
612 other trace elements in the North Atlantic Ocean: Observations from the A16N CLIVAR/CO2repeat
613 hydrography section, Mar. Chem., 120(1–4), 57–70, doi:10.1016/j.marchem.2008.08.003, 2010.

614 Cacador, I., Vale, C. and Catarino, F.: The influence of plants on concentration and fractionation of Zn, Pb, and
615 Cu in salt marsh sediments (Tagus Estuary, Portugal), J. Aquat. Ecosyst. Heal., 5(3), 193–198,
616 doi:10.1007/BF00124106, 1996.

617 Collier, R. and Edmond, J.: The trace element geochemistry of marine biogenic particulate matter, Prog.
618 Oceanogr., 13(2), 113–199, doi:10.1016/0079-6611(84)90008-9, 1984.

619 Cullen, J. T., Chong, M. and Ianson, D.: British columbian continental shelf as a source of dissolved iron to the
620 subarctic northeast Pacific Ocean, Global Biogeochem. Cycles, 23(4), 1–12, doi:10.1029/2008GB003326, 2009.

621 Cutter, G. A. and Bruland, K. W.: Rapid and noncontaminating sampling system for trace elements in global
622 ocean surveys, Limnol. Oceanogr. Methods, 10(JUNE), 425–436, doi:10.4319/lom.2012.10.425, 2012.

623 Dammshäuser, A., Wagener, T., Garbe-Schönberg, D. and Croot, P.: Particulate and dissolved aluminum and
624 titanium in the upper water column of the Atlantic Ocean, Deep. Res. Part I Oceanogr. Res. Pap., 73, 127–139,
625 doi:10.1016/j.dsr.2012.12.002, 2013.

626 Dehairs, F., Jacquet, S., Savoye, N., Van Mooy, B. A. S., Buesseler, K. O., Bishop, J. K. B., Lamborg, C. H.,
627 Elskens, M., Baeyens, W., Boyd, P. W., Casciotti, K. L. and Monnin, C.: Barium in twilight zone suspended
628 matter as a potential proxy for particulate organic carbon remineralization: Results for the North Pacific, Deep.
629 Res. Part II Top. Stud. Oceanogr., 55(14–15), 1673–1683, doi:10.1016/j.dsr2.2008.04.020, 2008.

630 Duarte, B., Silva, G., Costa, J. L., Medeiros, J. P., Azeda, C., Sá, E., Metelo, I., Costa, M. J. and Caçador, I.:
631 Heavy metal distribution and partitioning in the vicinity of the discharge areas of Lisbon drainage basins (Tagus
632 Estuary, Portugal), J. Sea Res., 93(February), 101–111, doi:10.1016/j.seares.2014.01.003, 2014.

633 Dutay, J. C., Tagliabue, A., Kriest, I. and van Hulten, M. M. P.: Modelling the role of marine particle on large
634 scale 231Pa, 230Th, Iron and Aluminium distributions, Prog. Oceanogr., 133, 66–72,
635 doi:10.1016/j.pocean.2015.01.010, 2015.

636 Dutkiewicz, A., Müller, R. D., O'Callaghan, S. and Jónasson, H.: Census of seafloor sediments in the world's
637 ocean, Geology, 43(9), 795–798, doi:10.1130/G36883.1, 2015.

638 Eittreim, S., Thorndike, E. M. and Sullivan, L.: Turbidity distribution in the Atlantic Ocean, Deep. Res.
639 Oceanogr. Abstr., 23(12), 1115–1127, doi:10.1016/0011-7471(76)90888-3, 1976.

640 Elderfield, H. and Schultz, A.: Mid-Ocean Ridge Hydrothermal Fluxes and the Chemical Composition of the
641 Ocean, Annu. Rev. Earth Planet. Sci., 24(1), 191–224, doi:10.1146/annurev.earth.24.1.191, 1996.

Ellwood, M. J., Nodder, S. D., King, A. L., Hutchins, D. A., Wilhelm, S. W. and Boyd, P. W.: Pelagic iron cycling during the subtropical spring bloom, east of New Zealand, Mar. Chem., 160, 18–33, doi:10.1016/j.marchem.2014.01.004, 2014.

Elrod, V. A., Berelson, W. M., Coale, K. H. and Johnson, K. S.: The flux of iron from continental shelf sediments: A missing source for global budgets, Geophys. Res. Lett., 31(12), 2–5, doi:10.1029/2004GL020216, 2004.

Fitzwater, S. E., Johnson, K. S., Gordon, R. M., Coale, K. H. and Smith, W. O.: Trace metal concentrations in athe Ross Sea and their relationship with nutrients and phytoplankton growth, Deep. Res. Part II Top. Stud. Oceanogr., 47(15–16), 3159–3179, doi:10.1016/S0967-0645(00)00063-1, 2000.

Fragoso, G. M., Poulton, A. J., Yashayaev, I. M., Head, E. J. H., Stinchcombe, M. C. and Purdie, D. A.: Biogeographical patterns and environmental controls of phytoplankton communities from contrasting hydrographical zones of the Labrador Sea, Prog. Oceanogr., 141, 212–226, doi:10.1016/j.pocean.2015.12.007, 2016.

Frew, R. D., Hutchins, D. A., Nodder, S., Sanudo-Wilhelmy, S., Tovar-Sanchez, A., Leblanc, K., Hare, C. E. and Boyd, P. W.: Particulate iron dynamics during FeCycle in subantarctic waters southeast of New Zealand, Global Biogeochem. Cycles, 20(1), 1–15, doi:10.1029/2005GB002558, 2006.

García-Ibáñez, M. I., Pardo, P. C., Carracedo, L. I., Mercier, H., Lherminier, P., Ríos, A. F. and Pérez, F. F.: Structure, transports and transformations of the water masses in the Atlantic Subpolar Gyre, Prog. Oceanogr., 135, 18–36, doi:10.1016/j.pocean.2015.03.009, 2015.

Gardner, W. D., Tucholke, B. E., Richardson, M. J. and Biscaye, P. E.: Benthic storms, nepheloid layers, and linkage with upper ocean dynamics in the western North Atlantic, Mar. Geol., 385, 304–327, doi:10.1016/j.margeo.2016.12.012, 2017.

Gardner, W. D., Richardson, M. J. and Mishonov, A. V.: Global assessment of benthic nepheloid layers and linkage with upper ocean dynamics, Earth Planet. Sci. Lett., 482, 126–134, doi:10.1016/j.epsl.2017.11.008, 2018.

Gerringa, L. J. A., Rijkenberg, M. J. A., Schoemann, V., Laan, P. and de Baar, H. J. W.: Organic complexation of iron in the West Atlantic Ocean, Mar. Chem., 177, 434–446, doi:10.1016/j.marchem.2015.04.007, 2015.

Hawkings, J. R., Wadham, J. L., Tranter, M., Raiswell, R., Benning, L. G., Statham, P. J., Tedstone, A., Nienow, P., Lee, K. and Telling, J.: Ice sheets as a significant source of highly reactive nanoparticulate iron to the oceans, Nat. Commun., 5(May), 1–8, doi:10.1038/ncomms4929, 2014.

Hwang, J., Druffel, E. R. M. and Eglinton, T. I.: Widespread influence of resuspended sediments on oceanic particulate organic carbon: Insights from radiocarbon and aluminum contents in sinking particles, Global Biogeochem. Cycles, 24(4), 1–10, doi:10.1029/2010GB003802, 2010.

675 Jeandel, C. and Oelkers, E. H.: The influence of terrigenous particulate material dissolution on ocean chemistry
676 and global element cycles, Chem. Geol., 395, 50–66, doi:10.1016/j.chemgeo.2014.12.001, 2015.

677 Jeandel, C., Peucker-Ehrenbrink, B., Jones, M. T., Pearce, C. R., Oelkers, E. H., Godderis, Y., Lacan, F.,
678 Aumont, O. and Arsouze, T.: Ocean margins: The missing term in oceanic element budgets?, Eos, Transactions
679 American Geophysical Union, 92(26), 217–224, doi: 10.1029/2011EO260001, 2011.

680 Jickells, T. D., An, Z. S., Andersen, K. K., Baker, A. R., Bergametti, C., Brooks, N., Cao, J. J., Boyd, P. W.,
681 Duce, R. A., Hunter, K. A., Kawahata, H., Kubilay, N., LaRoche, J., Liss, P. S., Mahowald, N., Prospero, J. M.,
682 Ridgwell, A. J., Tegen, I. and Torres, R.: Global iron connections between desert dust, ocean biogeochemistry,
683 and climate, Science (80-.)., 308(5718), 67–71, doi:10.1126/science.1105959, 2005.

684 Jouanneau, J. M., Garcia, C., Oliveira, A., Rodrigues, A., Dias, J. A. and Weber, O.: Dispersal and deposition of
685 suspended sediment on the shelf off the Tagus and Sado estuaries, S.W. Portugal, Prog. Oceanogr., 42(1–4),
686 233–257, doi:10.1016/S0079-6611(98)00036-6, 1998.

687 Labatut, M., Lacan, F., Pradoux, C., Chmeleff, J., Radic, A., Murray, J. W., Poitrasson, F., Johansen, A. M.,
688 Thil, F., Lacan, F., Pradoux, C., Chmeleff, J., Radic, A., Murray, J. W., Poitrasson, F., Johansen, A. M. and
689 Thil, F.: Iron sources and dissolved - particulate interactions in the seawater of the Western Equatorial Pacific,
690 iron isotope perspectives., Global Biogeochemical Cycles, 1044–1065, doi:10.1002/2014GB004928, 2014.

691 Lam, P. J. and Bishop, J. K. B.: The continental margin is a key source of iron to the HNLC North Pacific
692 Ocean, Geophys. Res. Lett., 35(7), 1–5, doi:10.1029/2008GL033294, 2008.

693 Lam, P. J., Ohnemus, D. C. and Marcus, M. A.: The speciation of marine particulate iron adjacent to active and
694 passive continental margins, Geochim. Cosmochim. Acta, 80, 108–124, doi:10.1016/j.gca.2011.11.044, 2012.

695 Lam, P. J., Ohnemus, D. C. and Auro, M. E.: Size-fractionated major particle composition and concentrations
696 from the US GEOTRACES North Atlantic Zonal Transect, Deep. Res. Part II Top. Stud. Oceanogr., 116, 303–
697 320, doi:10.1016/j.dsr2.2014.11.020, 2015.

698 Lam, P. J., Lee, J. M., Heller, M. I., Mehic, S., Xiang, Y. and Bates, N. R.: Size-fractionated distributions of
699 suspended particle concentration and major phase composition from the U.S. GEOTRACES Eastern Pacific
700 Zonal Transect (GP16), Mar. Chem., (April), 0–1, doi:10.1016/j.marchem.2017.08.013, 2017.

701 Lannuzel, D., Bowie, A. R., van der Merwe, P. C., Townsend, A. T. and Schoemann, V.: Distribution of
702 dissolved and particulate metals in Antarctic sea ice, Mar. Chem., 124(1–4), 134–146,
703 doi:10.1016/j.marchem.2011.01.004, 2011.

704 Lannuzel, D., Van der Merwe, P. C., Townsend, A. T. and Bowie, A. R.: Size fractionation of iron, manganese
705 and aluminium in Antarctic fast ice reveals a lithogenic origin and low iron solubility, Mar. Chem., 161, 47–56,
706 doi:10.1016/j.marchem.2014.02.006, 2014.

Lee, J. M., Heller, M. I. and Lam, P. J.: Size distribution of particulate trace elements in the U.S. GEOTRACES Eastern Pacific Zonal Transect (GP16), Mar. Chem., 201(September 2017), 108–123, doi:10.1016/j.marchem.2017.09.006, 2017.

Lemaître, N., planquette, H., Planchon, F., Sarthou, G., Jacquet, S., Garcia-Ibanez, M. I., Gourain, A., Cheize, M., Monin, L., Andre, L., Laha, P., Terryn, H., and Dehairs, F.: Particulate barium tracing significant mesopelagic carbon remineralisation in the North Atlantic, Biogeosciences Discussions, doi:10.5194/bg-15-2289-2018, 2018a.

Lemaitre, N., Planchon, F., Planquette, H., Dehairs, F., Fonseca-Batista, D., Roukaerts, A., Deman, F., Tang, Y., Mariez, C., and Sarthou G.: High variability of export fluxes along the North Atlantic GEOTRACES section GA01: Particulate organic carbon export deduced from the 234Th method, Biogeosciences Discuss., doi:10.5194/bg-2018-190, 2018b.

Le Roy, E., Sanial, V., Charette, M.A., Van Beek, P., Lacan, F., Jacquet, S.H., Henderson, P.B., Souhaut, M., García-Ibáñez, M.I., Jeandel, C. and Pérez, F.: The 226Ra-Ba relationship in the North Atlantic during GEOTRACES-GA01, Biogeosciences Discussions, doi:10.5194/bg-2017-478, 2017.

Loring, D. H. and Asmund, G.: Geochemical factors controlling accumulation of major and trace elements in Greenland coastal and fjord sediments, Environ. Geol., 28(1), 2–11, doi:10.1007/s002540050072, 1996.

Mahowald, N. M., Baker, A. R., Bergametti, G., Brooks, N., Duce, R. A., Jickells, T. D., Kubilay, N., Prospero, J. M. and Tegen, I.: Atmospheric global dust cycle and iron inputs to the ocean, Global Biogeochem. Cycles, 19(4), doi:10.1029/2004GB002402, 2005.

Marsay, C. M., Lam, P. J., Heller, M. I., Lee, J. M. and John, S. G.: Distribution and isotopic signature of ligand-leachable particulate iron along the GEOTRACES GP16 East Pacific Zonal Transect, Mar. Chem., (November 2016), 1–14, doi:10.1016/j.marchem.2017.07.003, 2017.

Martin, J. H., Fitzwater, S. E., Michael Gordon, R., Hunter, C. N. and Tanner, S. J.: Iron, primary production and carbon-nitrogen flux studies during the JGOFS North Atlantic bloom experiment, Deep. Res. Part II, 40(1–2), 115–134, doi:10.1016/0967-0645(93)90009-C, 1993.

McCave, I. N. and Hall, I. R.: Turbidity of waters over the Northwest Iberian continental margin, Prog. Oceanogr., 52(2–4), 299–313, doi:10.1016/S0079-6611(02)00012-5, 2002.

Menzel Barraqueta, J.L., Schlosser, C., Planquette, H., Gourain, A., Cheize, M., Boutorh, J., Shelley, R., Pereira Contreira, L., Gledhill, M., Hopwood, M.J. and Lherminier, P.: Aluminium in the North Atlantic Ocean and the Labrador Sea (GEOTRACES GA01 section): roles of continental inputs and biogenic particle removal. Biogeosciences Discussions, 1-28, doi: 10.5194/bg-2018-39, 2018.

738 Milne, A., Schlosser, C., Wake, B. D., Achterberg, E. P., Chance, R., Baker, A. R., Forryan, A. and Lohan, M.
739 C.: Particulate phases are key in controlling dissolved iron concentrations in the (sub)tropical North Atlantic,
740 Geophys. Res. Lett., 44(5), 2377–2387, doi:10.1002/2016GL072314, 2017.

741 Mudie, P. J., Keen, C. E., Hardy, I. A. and Vilks, G.: Multivariate analysis and quantitative paleoecology of
742 benthic foraminifera in surface and Late Quaternary shelf sediments, northern Canada, Mar. Micropaleontol.,
743 8(4), 283–313, doi:10.1016/0377-8398(84)90018-5, 1984.

744 Nuester, J., Shema, S., Vermont, A., Fields, D. M. and Twining, B. S.: The regeneration of highly bioavailable
745 iron by meso- and microzooplankton, , 59(4), 1399–1409, doi:10.4319/lo.2014.59.4.1399, 2014.

746 Oelkers, E. H., Jones, M. T., Pearce, C. R., Jeandel, C., Eiriksdottir, E. S. and Gislason, S. R.: Riverine
747 particulate material dissolution in seawater and its implications for the global cycles of the elements, Geosci.,
748 344(11–12), 646–651, doi:10.1016/j.crte.2012.08.005, 2012.

749 Ohnemus, D. C. and Lam, P. J.: Cycling of lithogenic marine particles in the US GEOTRACES North Atlantic
750 transect, Deep. Res. Part II Top. Stud. Oceanogr., 116, 283–302, doi:10.1016/j.dsr2.2014.11.019, 2015.

751 Peers, G. and Price, N. M.: A role for manganese in superoxide dismutases and growth of iron-deficient
752 diatoms, Limnol. Oceanogr., 49(5), 1774–1783, doi:10.4319/lo.2004.49.5.1774, 2004.

753 Planquette, H. and Sherrell, R. M.: Sampling for particulate trace element determination using water sampling
754 bottles: Methodology and comparison to in situ pumps, Limnol. Oceanogr. Methods, 10(5), 367–388,
755 doi:10.4319/lom.2012.10.367, 2012.

756 Planquette, H., Fones, G. R., Statham, P. J. and Morris, P. J.: Origin of iron and aluminium in large particles (>
757 53 μm) in the Crozet region, Southern Ocean, Mar. Chem., 115(1–2), 31–42,
758 doi:10.1016/j.marchem.2009.06.002, 2009.

759 Planquette, H., Sanders, R. R., Statham, P. J., Morris, P. J. and Fones, G. R.: Fluxes of particulate iron from the
760 upper ocean around the Crozet Islands: A naturally iron-fertilized environment in the Southern Ocean, Global
761 Biogeochem. Cycles, 25(2), doi:10.1029/2010GB003789, 2011.

762 Planquette, H., Sherrell, R. M., Stammerjohn, S. and Field, M. P.: Particulate iron delivery to the water column
763 of the Amundsen Sea, Antarctica, Mar. Chem., 153, 15–30, doi:10.1016/j.marchem.2013.04.006, 2013.

764 Radic, A., Lacan, F. and Murray, J. W.: Iron isotopes in the seawater of the equatorial Pacific Ocean: New
765 constraints for the oceanic iron cycle, Earth Planet. Sci. Lett., 306(1–2), 1–10, doi:10.1016/j.epsl.2011.03.015,
766 2011.

767 Raiswell, R., Benning, L. G., Tranter, M. and Tulaczyk, S.: Bioavailable iron in the Southern Ocean: The
768 significance of the iceberg conveyor belt, Geochem. Trans., 9(1), 7, doi:10.1186/1467-4866-9-7, 2008.

769 Rijkenberg, M. J. A., Middag, R., Laan, P., Gerringa, L. J. A., Van Aken, H. M., Schoemann, V., De Jong, J. T.
770 M. and De Baar, H. J. W.: The distribution of dissolved iron in the West Atlantic Ocean, PLoS One, 9(6), 1–14,
771 doi:10.1371/journal.pone.0101323, 2014.

772 Rutgers Van Der Loeff, M. M., Meyer, R., Rudels, B. and Rachor, E.: Resuspension and particle transport in the
773 benthic nepheloid layer in and near Fram Strait in relation to faunal abundances and 234Th depletion, Deep.
774 Res. Part I Oceanogr. Res. Pap., 49(11), 1941–1958, doi:10.1016/S0967-0637(02)00113-9, 2002.

775 Sanders, R., Henson, S. A., Koski, M., De La Rocha, C. L., Painter, S. C., Poulton, A. J., Riley, J., Salihoglu, B.,
776 Visser, A., Yool, A., Bellerby, R. and Martin, A. P.: The Biological Carbon Pump in the North Atlantic, Prog.
777 Oceanogr., 129(PB), 200–218, doi:10.1016/j.pocean.2014.05.005, 2014.

778 Sarthou, G., Vincent, D., Christaki, U., Obernosterer, I., Timmermans, K. R. and Brussaard, C. P. D.: The fate
779 of biogenic iron during a phytoplankton bloom induced by natural fertilisation: Impact of copepod grazing,
780 Deep. Res. Part II Top. Stud. Oceanogr., 55(5–7), 734–751, doi:10.1016/j.dsr2.2007.12.033, 2008.

781 Schlosser, C., Schmidt, K., Aquilina, A., Homoky, W. B., Castrillejo, M., Mills, R. A., Patey, M. D., Fielding,
782 S., Atkinson, A. and Achterberg, E. P.: Mechanisms of dissolved and labile particulate iron supply to shelf
783 waters and phytoplankton blooms off South Georgia, Southern Ocean, Biogeosciences Discuss., 0049(July), 1–
784 49, doi:10.5194/bg-2017-299, 2017.

785 Shelley, R. U., Landing, W. M., Ussher, S. J., Planquett, H. and Sarthou, G.: Characterisation of aerosol
786 provenance from the fractional solubility of Fe (Al, Ti, Mn, Co, Ni, Cu, Zn , Cd and Pb) in North Atlantic
787 aerosols (GEOTRACES GA01 and GA03), Biogeosciencess, submitted(November), 1–31, doi:10.5194/bg-
788 2017-415, 2017.

789 Shelley, R. U., Landing, W. M., Ussher, S. J., Planquette, H. and Sarthou, G.: Regional trends in the fractional
790 solubility of Fe and other metals from North Atlantic aerosols (GEOTRACES cruises GA01 and GA03)
791 following a two-stage leach, Biogeosciences, 155194(1), 2271–2288, doi:10.5194/bg-15-2271-2018, 2018.

792 Sherrell, R. M., Field, P. M. and Gao, Y.: Temporal variability of suspended mass and composition in the
793 Northeast Pacific water column: Relationships to sinking flux and lateral advection, Deep. Res. Part II Top.
794 Stud. Oceanogr., 45(4–5), 733–761, doi:10.1016/S0967-0645(97)00100-8, 1998.

795 Spinrad, R. W.,Zaneveld, J. R. and Kitchen, J.C.: A Study of the Optical Characteristics of the Suspended
796 Particles Benthic N epheloid Layer of the Scotian Rise, J. Geophys. Res., 88, 7641–7645, doi:0148-
797 0227/83/003C, 1983.

798 Statham, P. J., Skidmore, M. and Tranter, M.: Inputs of glacially derived dissolved and colloidal iron to the
799 coastal ocean and implications for primary productivity, Global Biogeochem. Cycles, 22(3), 1–11,
800 doi:10.1029/2007GB003106, 2008.

Straneo, F., Pickart, R. S. and Lavender, K.: Spreading of Labrador sea water: An advective-diffusive study based on Lagrangian data, Deep. Res. Part I Oceanogr. Res. Pap., 50(6), 701–719, doi:10.1016/S0967-0637(03)00057-8, 2003.

Sunda, W. G. and Huntsman, S. A.: Effect of Competitive Interactions Between Manganese and Copper on Cellular Manganese and Growth in Estuarine and Oceanic Species of the Diatom Thalassiosira, Limnol. Oceanogr., 28(5), 924–934, doi:10.4319/lo.1983.28.5.0924, 1983.

Tagliabue, A., Bopp, L., Dutay, J. C., Bowie, A. R., Chever, F., Jean-Baptiste, P., Bucciarelli, E., Lannuzel, D., Remenyi, T., Sarthou, G., Aumont, O., Gehlen, M. and Jeandel, C.: Hydrothermal contribution to the oceanic dissolved iron inventory, Nat. Geosci., 3(4), 252–256, doi:10.1038/ngeo818, 2010.

Tagliabue, A., Bowie, A. R., Boyd, P. W., Buck, K. N., Johnson, K. S. and Saito, M. A.: The integral role of iron in ocean biogeochemistry, Nature, 543(7643), 51–59, doi:10.1038/nature21058, 2017.

Taylor, S. . and McLennan, S. .: The geochemical evolution of the continental crust, Rev. Geophys., 33(2), 241–265, doi:10.1029/95RG00262, 1995.

Tebo, B. M. and Emerson, S. R.: Effect of Oxygen Tension Manganese (II) Concentration and Temperature on the Microbially Catalyzed Manganese-Ii Oxidation Rate in a Marine Fjord, Appl. Environ. Microbiol., 50(5), 1268–1273, 1985.

Tebo, B. M., Nealson, K. H., Emerson, S. and Jacobs, L.: Microbial mediation of Mn(II) and Co(II) precipitation at the o2/H2S interfaces in two anoxic fjords, 29(6), 1247–1258, 1984.

Tonnard, M., Planquette, H., Bowie, A. R., van der Merwe, P., Gallinari, M., Desprez de Gésincourt, F., Germain, Y., Gourain, A., Benetti, M., Reverdin, G., Tréguer, P., Boutorh, J., Cheize, M., Menzel Barraqueta, J., Pereira-Contreira, L., Shelley, R., Lherminier, P., and Sarthou, G.: Dissolved iron in the North Atlantic Ocean and Labrador Sea along the GEOVIDE section (GEOTRACES section GA01), Biogeosciences Discuss., https://doi.org/10.5194/bg-2018-147, 2018

Trefry, J. H., Trocine, R. P., Klinkhammer, G. P. and Rona, P. A.: Iron and copper enrichment of suspended particles in dispersed hydrothermal plumes along the mid???Atlantic Ridge, Geophys. Res. Lett., 12(8), 506–509, doi:10.1029/GL012i008p00506, 1985.

Ussher, S. J., Achterberg, E. P. and Worsfold, P. J.: Marine biogeochemistry of iron, Environ. Chem., 1(2), 67–80, doi:10.1071/EN04053, 2004.

Ussher, S. J., Worsfold, P. J., Achterberg, E. P., Laës, A., Blain, S., Laan, P., de Baar, H. J. W.: Distribution and redox speciation of dissolved iron on the European continental margin, Limnol. Oceanogr., 52(6), 2530–2539, doi:10.4319/lo.2007.52.6.2530, 2007.

Van der Merwe, P., Lannuzel, D., Bowie, A. R., Mancuso Nichols, C. A. and Meiners, K. M.: Iron fractionation in pack and fast ice in East Antarctica: Temporal decoupling between the release of dissolved and particulate

iron during spring melt, Deep. Res. Part II Top. Stud. Oceanogr., 58(9–10), 1222–1236, doi:10.1016/j.dsr2.2010.10.036, 2011a.

Van Der Merwe, P., Lannuzel, D., Bowie, A. R. and Meiners, K. M.: High temporal resolution observations of spring fast ice melt and seawater iron enrichment in East Antarctica, J. Geophys. Res. Biogeosciences, 116(3), 1–18, doi:10.1029/2010JG001628, 2011b.

Weinstein, S. E. and Moran, S. B.: Distribution of size-fractionated particulate trace metals collected by bottles and in-situ pumps in the Gulf of Maine-Scotian Shelf and Labrador Sea, Mar. Chem., 87(3–4), 121–135, doi:10.1016/j.marchem.2004.02.004, 2004.

Yashayaev, I.: Hydrographic changes in the Labrador Sea, 1960-2005, Prog. Oceanogr., 73(3–4), 242–276, doi:10.1016/j.pocean.2007.04.015, 2007.

Yashayaev, I. and Loder, J. W.: Enhanced production of Labrador Sea Water in 2008, Geophys. Res. Lett., 36(1), doi:10.1029/2008GL036162, 2009.

Zunino, P., Lherminier, P., Mercier, H., Daniault, N., García-Ibáñez, M. I., and Pérez, F. F.: The GEOVIDE cruise in May–June 2014 reveals an intense Meridional Overturning Circulation over a cold and fresh subpolar North Atlantic. Biogeosciences, 14(23), 5323, 2017.

Figure 1: Map of stations where suspended particle samples were collected with GO-FLO bottles during the GEOVIDE cruise (GA01). Biogeochemical provinces are indicated by red squares, IM: Iberian Margin, IAP: Iberian Abyssal Plain, WEB: Western European Basin, IcB: Iceland Basin, RR: Reykjanes Ridge, IrB: Irminger Basin, GS: Greenland Shelf, LB: Labrador Basin, NS: Newfoundland Shelf. This figure was generated by Ocean Data View (Schlitzer, R., Ocean Data View, odv.awi.de, 2017).

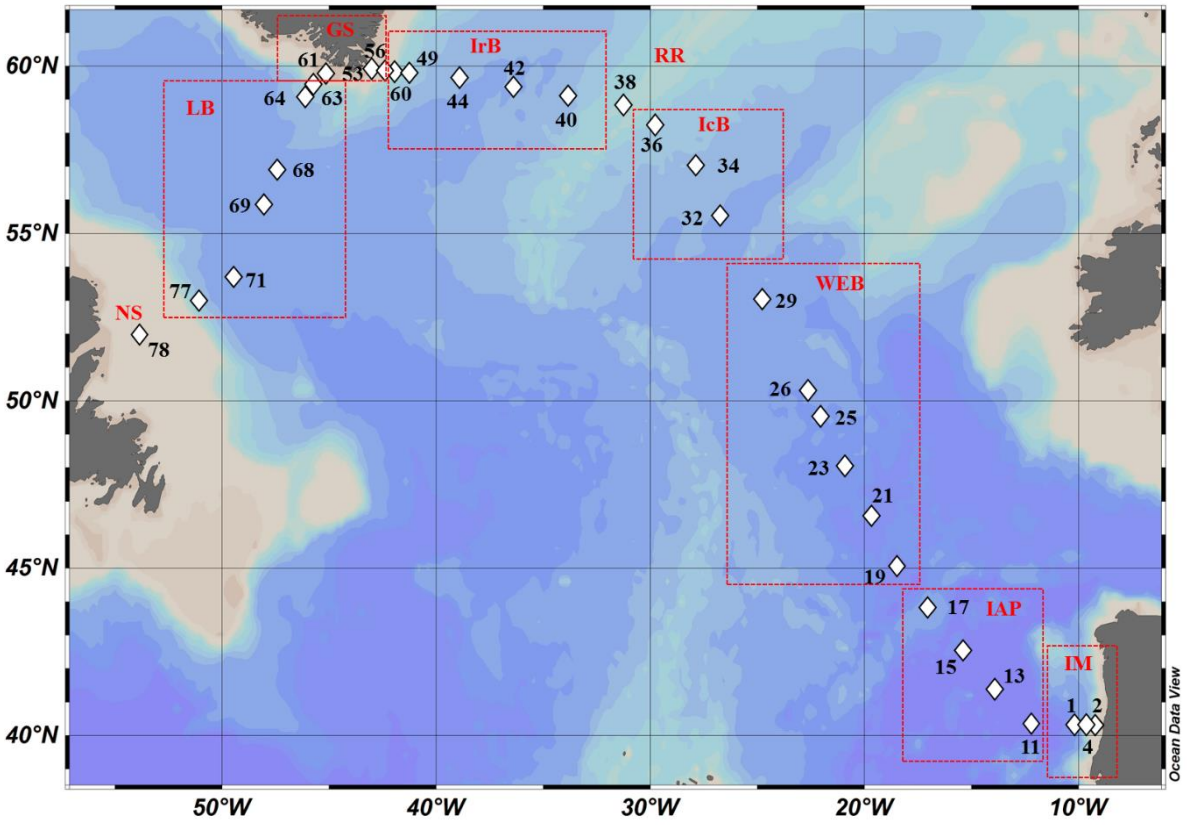

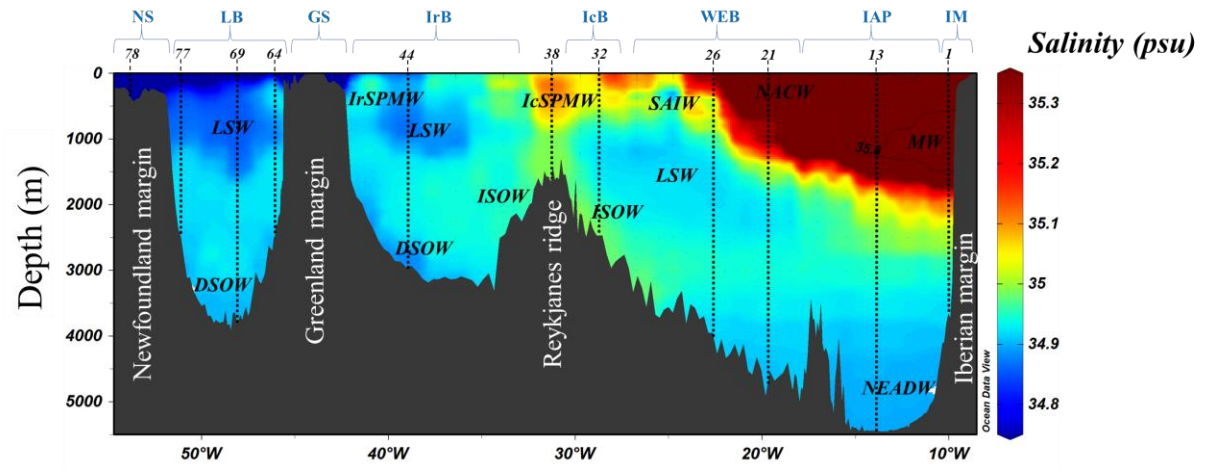

Figure 2: Salinity section during the GEOVIDE cruise. Water masses are indicated in black, MW: Mediterranean Water; NACW: North Atlantic Central Water; NEADW: North East Atlantic Deep Water; LSW: Labrador Sea Water; ISOW: Iceland-Scotland Overflow Water; SAIW: Sub-Arctic Intermediate Water; IcSPMW: Iceland Sub-Polar Mode Water; IrSPMW: Irminger Sub-Polar Mode Water. Stations locations are indicated by the numbers. Biogeochemical provinces are indicated in blue font above station numbers. Contour of salinity = 35.8psu have been apply to identify the Mediterranean Water. This figure was generated by Ocean Data View (Schlitzer, R., Ocean Data View, odv.awi.de, 2017).

Figure 3: Left) Distribution of total particulate iron (a, PFe), aluminium (b, PAl), manganese (c, PMn) and phosphorus (d, PP) concentrations (in nmol L^{-1}) along the GEOVIDE section. Right) Contribution of small size fraction (0,45-5 µm) expressed as percentage (%) of the total concentration of PFe (e), PAl (f), PMn (g) and PP (h). Station IDs and biogeochemical region are indicated on top of section a. This figure was generated by Ocean Data View (Schlitzer, R., Ocean Data View, odv.awi.de, 2017).

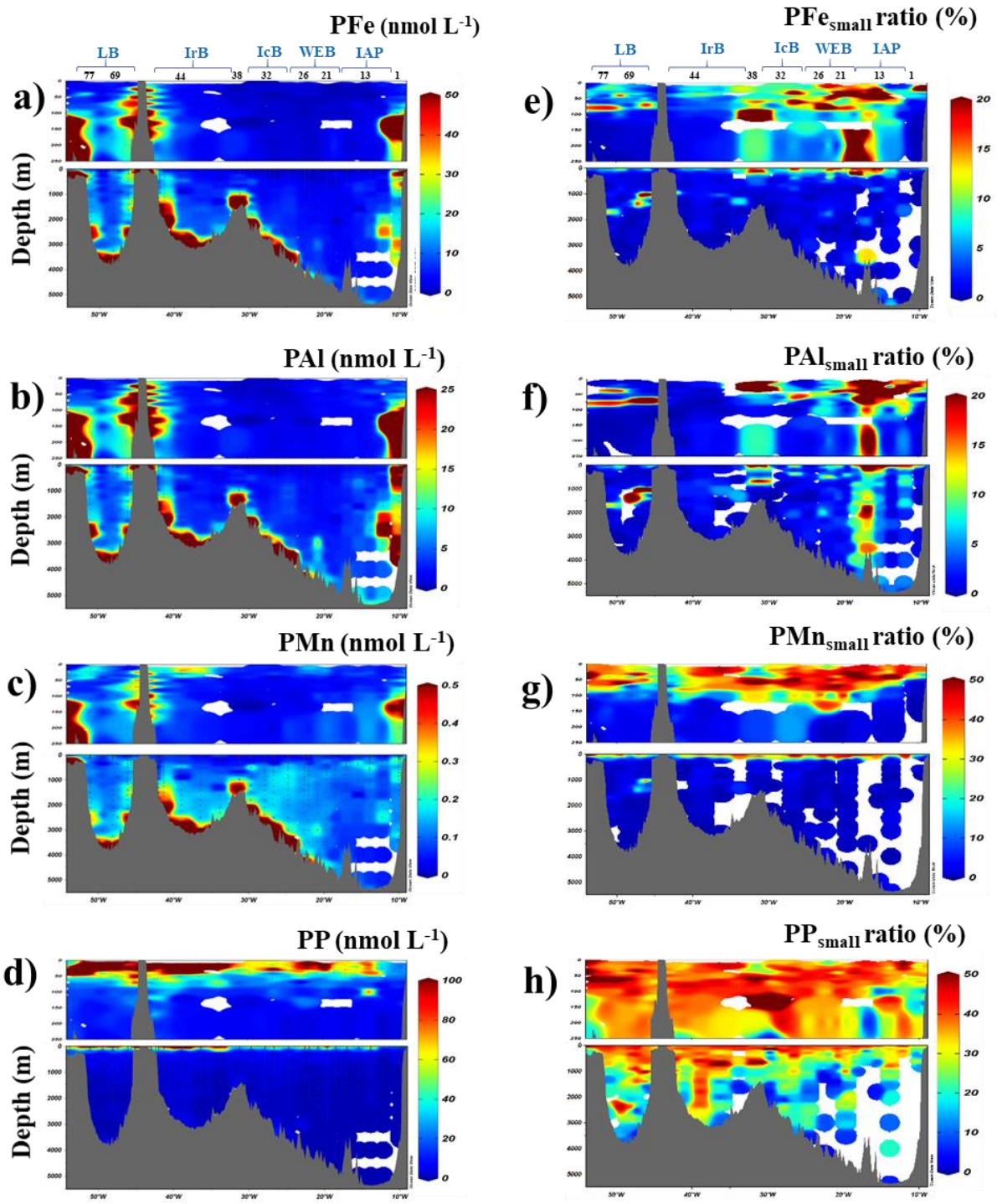

Figure 4: Boxplot figure of the particulate iron vertical profile (in nmol L^{-1}) in the a) Iberian abyssal plain (IAP), b) Western European basin (WEB), c) Icelandic basin (IcB), d) Irminger basin (IrB) and e) Labrador basins (LB). The left boundary of the box represents the 25th percentile while the right boundary represents the 75th percentile, the line within the box marks the median value. Whiskers represent the 90th and 10th percentiles and dots are the outlying data. Seven depth boxes have been used (0-100m, 100-200m, 200-500m, 500-1000m, 1000-2000m, 2000-3000m and 3000m-bottom depth).

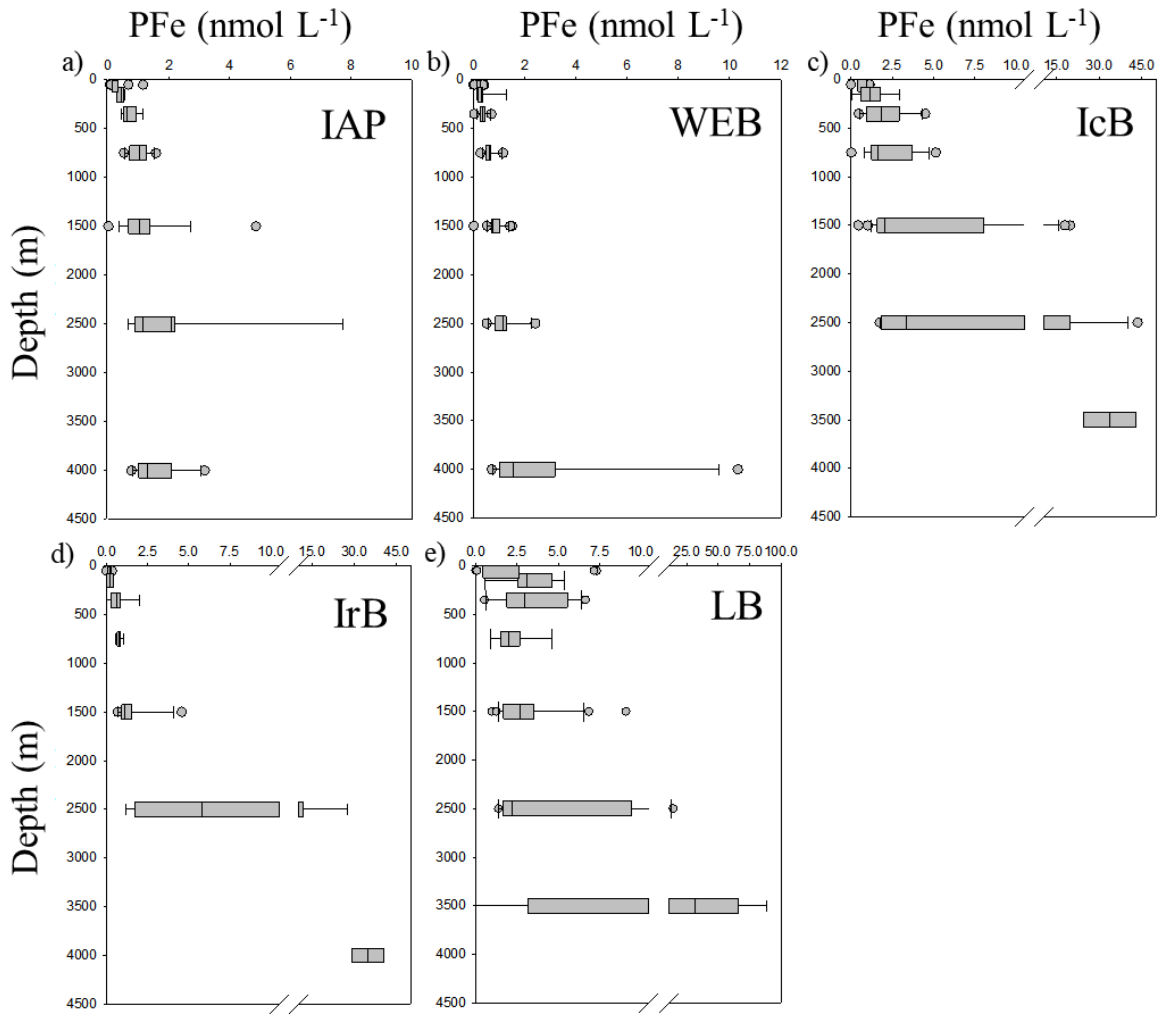

Figure 5: Factor fingerprint of the positive matrix factorisation. The four factors are represented in a stacked bar chart of the percentage of variance explained per element.

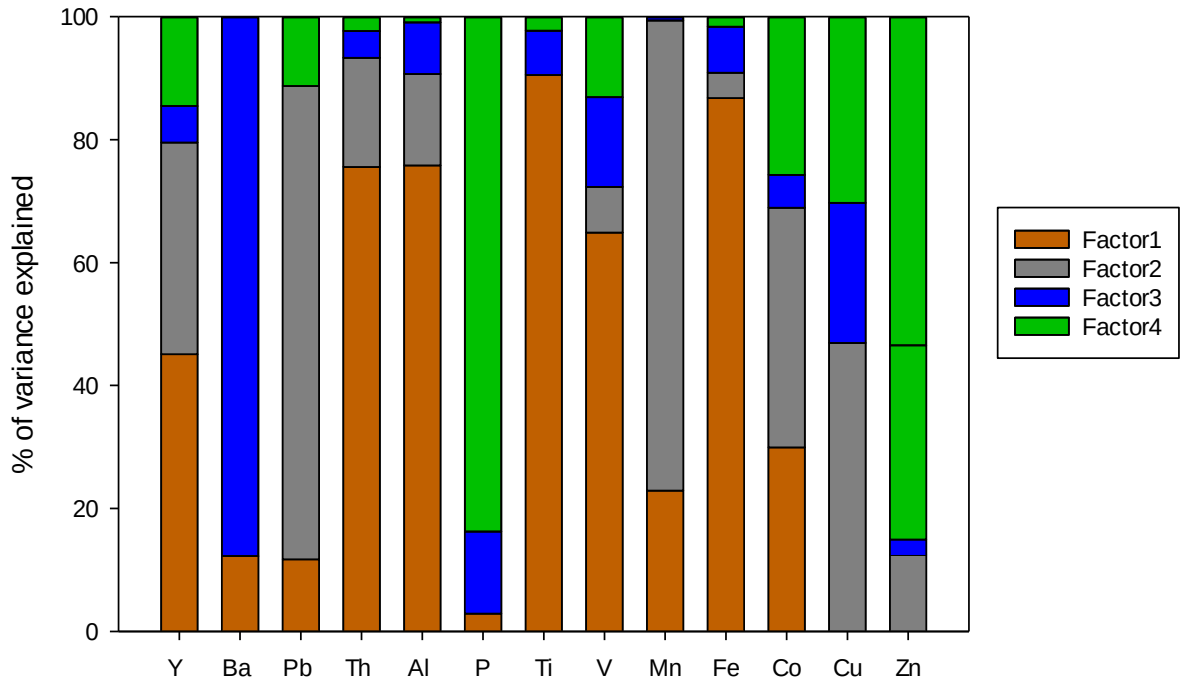

Figure 6: a) Section of the PFe to PAl molar ratio (mol mol^{-1}); (b) contribution of lithogenic PFe (%) based on Eq. (1). Station IDs and biogeochemical provinces are indicated above each section. This figure was generated by Ocean Data View (Schlitzer, R., Ocean Data View, odv.awi.de, 2017).

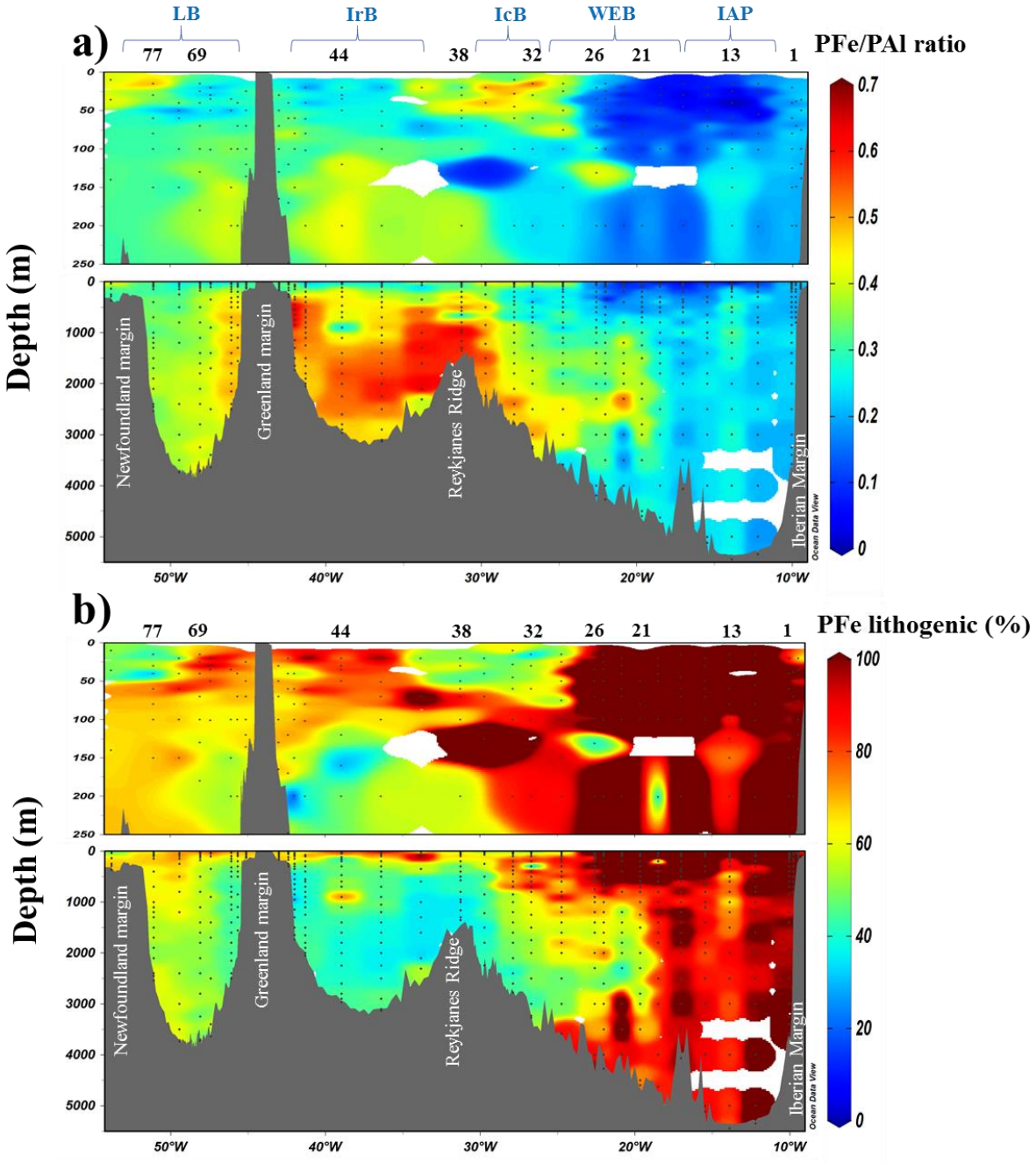

Figure 7: Whisker diagram of PFe/PAl molar ratio (mol mol^{-1}) in the different water masses sampled along the GA01 line. Median values for the water masses were as follows: LSW_{lb}= 0.37; LSW_{Ir}=0.44; LSW_{WEB}=0.36; $ISOW_{east}$=0.48; $ISOW_{west}$=0.58; $DSOW_{lab}$=0.42; $DSOW_{Ir}$=0.47; NEADW=0.23; MW=0.22 mol mol^{-1}.

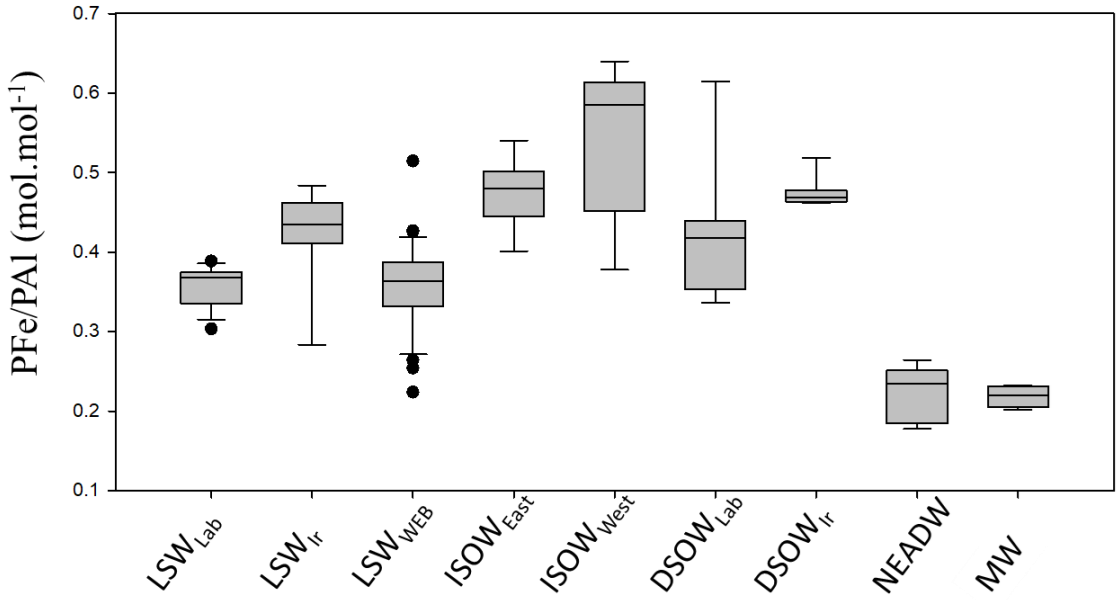

Figure 8: Scatter of the PFe/PAl ratio at the Iberian (red dots), East Greenland (black dots), West Greenland (green dots) and Newfoundland margins (blue dots). Dashed line indicate the UCC ratio (Taylor and McLennan, 1995).

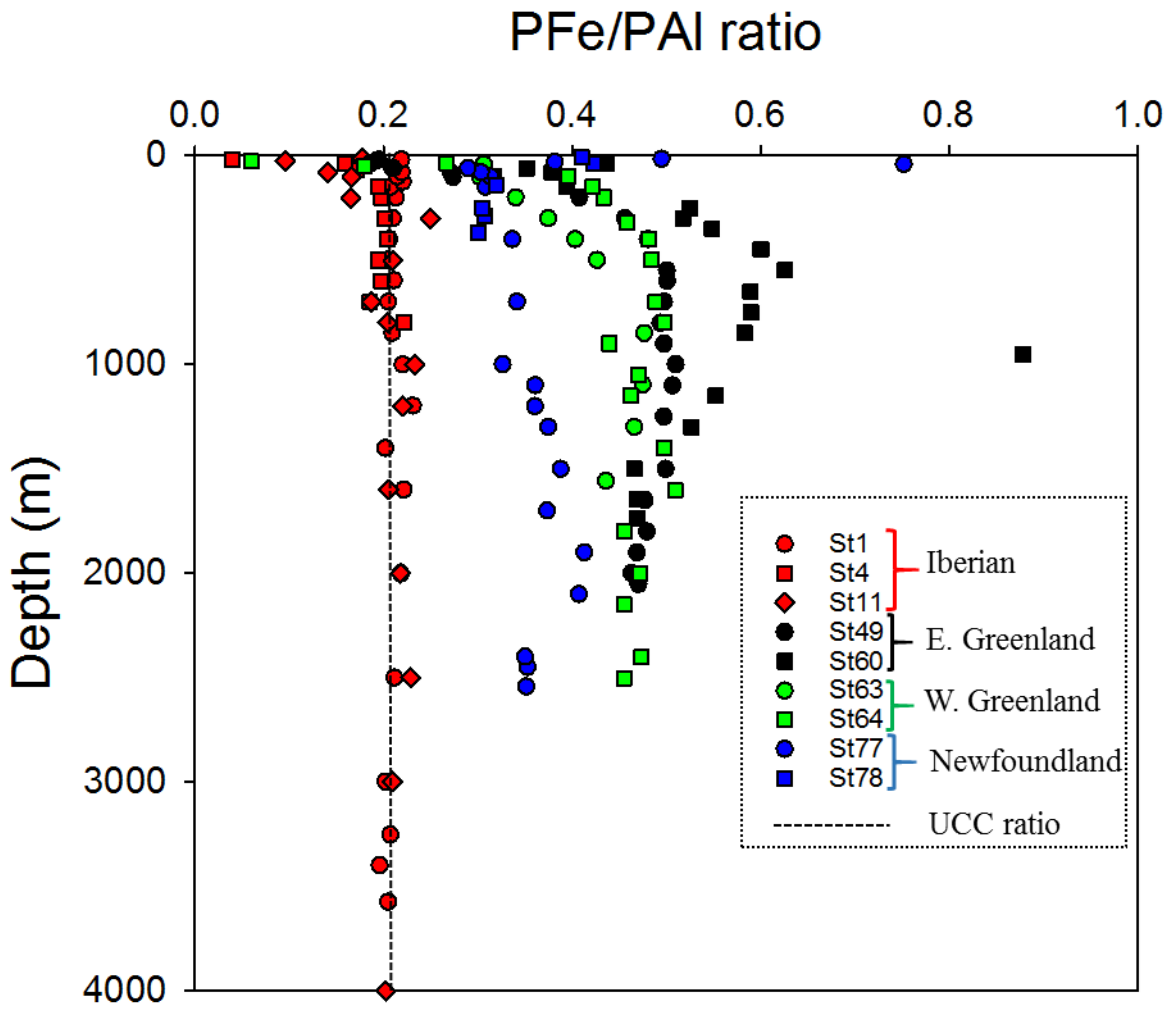

Figure 9: Section of derived contribution of sedimentary inputs manganese bulk sediment proxy (a) and transmissometry (b) along the GA01 section. Station IDs and biogeochemical region are indicated above the section (a). This figure was generated by Ocean Data View (Schlitzer, R., Ocean Data View, odv.awi.de, 2017).

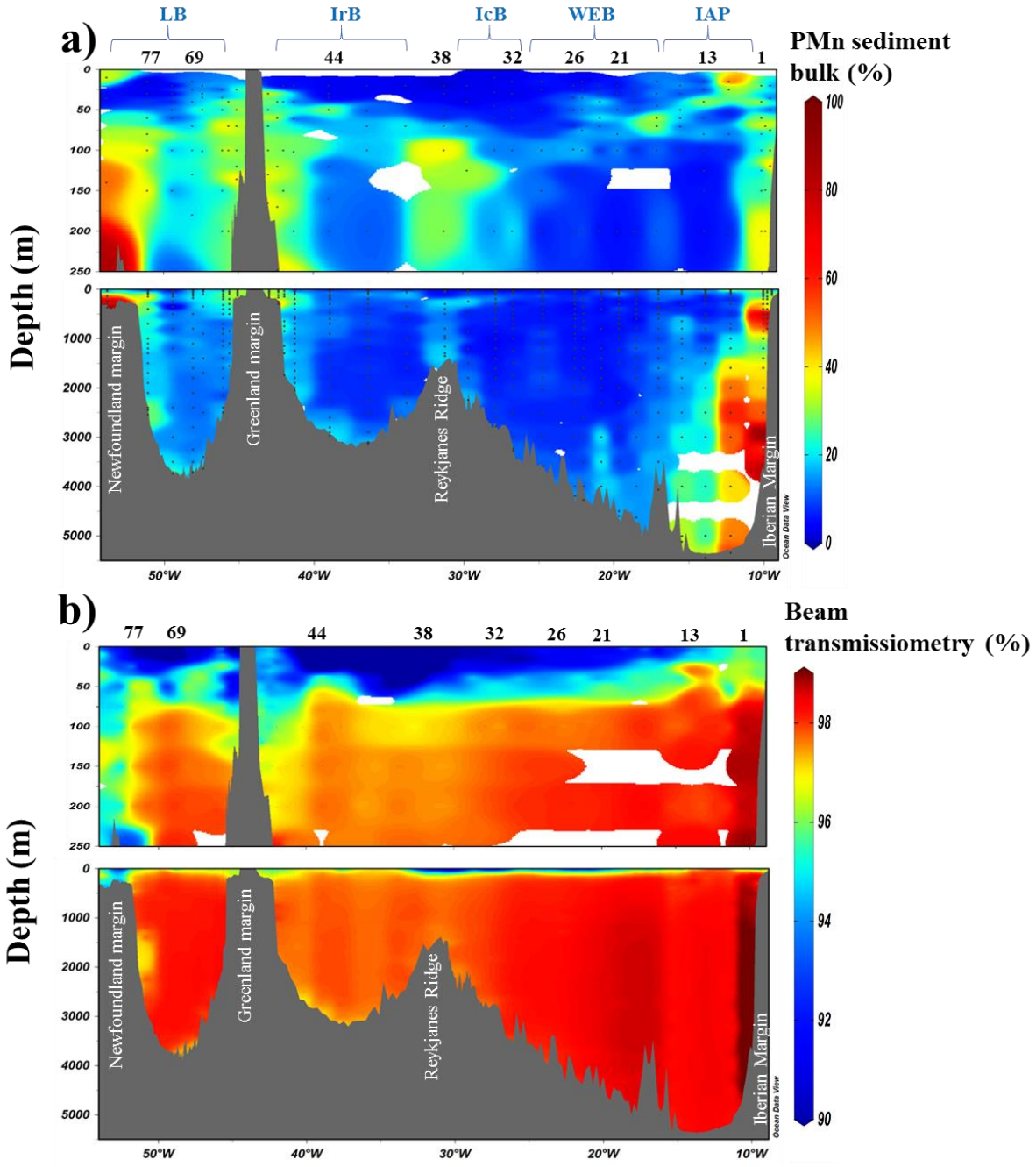

1029

1030

1031

1032

1033

1034

1035 **Figure 10: Vertical profiles of PFe (nmol L^{-1}, a), lithogenic proportion of particulate iron (%, b) and sedimentary**
1036 **proportion of particulate manganese (%, c) at the Iberian, East-West Greenland and Newfoundland margins.**

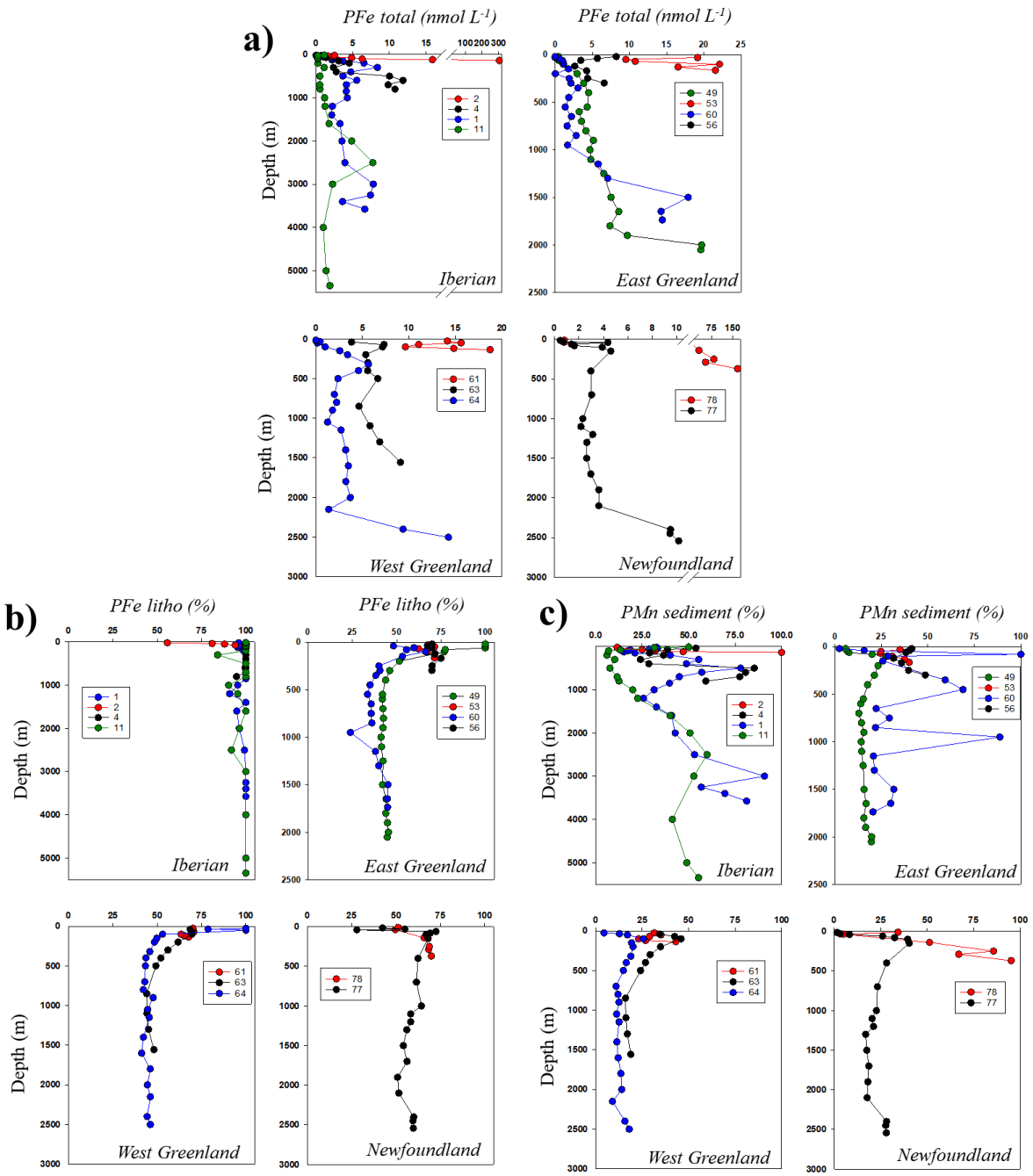

1037

1038

1039

1040

1041

1042

1043

1044 **Figure 11: PFe total (a); PFe/PAl ratio (b) and beam transmissometry (%) as a function of depth above the seafloor**
1045 **(m) at selected stations where a decrease in transmissometry was recorded.**

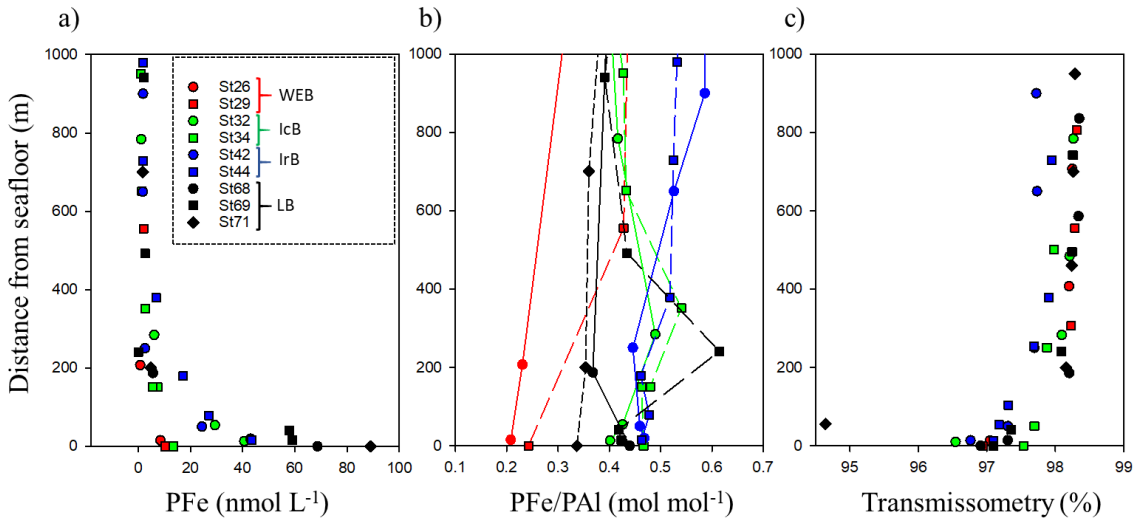
a)
b)
c)
Distance from seafloor (m)
PFe (nmol L-1)
PFe/PAl (mol mol-1)
Transmissometry (%)
St26
St29
St32
St34
St42
St44
St68
St69
St71
WEB
IcB
IrB
LB

		Fe	Al	P	Mn
Blank (nmol L^{-1})	5µm filter	0.072	0.100	0.511	0.003
	0.45µm filter	0.132	0.164	1.454	0.005
Limit of detection (nmol L^{-1})	5µm filter	0.011	0.030	0.365	0.001
	0.45µm filter	0.026	0.046	1.190	0.001
Recovery CRM (%)	BCR-414 (n=10)	88 ± 7			94 ± 7
	MESS-4 (n=5)	98 ± 14	97 ± 14	80 ± 30	110 ± 18
	PACS-3 (n=8)	101 ± 9	99 ± 14	91 ± 34	112 ± 11

Table 1: Blank and limit of detection (nmol L^{-1}) of the two filters and Certified reference material (CRM) recoveries during GEOVIDE suspended particle digestion.

Author	Year	Fraction	Location	Depth range	PFe	PAl	PMn	PP
This study		>0.45µm	N. Atlantic (>40°N)	All	bdl-304	bdl-1544	bdl-3.5	bdl-402
Barrett et al.	2012	0.4um	N. Atlantic (25-60°N)	Upper 1000m	0.29-1.71	0.2-19.7		
Dammshauser et al.	2013	>0.2 µm	Eastern tropical N.A.	0-200		0.59-17.7		
Dammshauser et al.	2013	>0.2 µm	Meridional Atlantic	0-200		0.35-16.1		
Lam et al.	2012	1–51 um	Eastern tropical N.A.	0-600	ND-12			
Lannuzel et al.	2011	>0.2 µm	East Antarctic	Surface		0.02-10.67	0.01-0.14	
Lannuzel et al.	2014	>0.2 µm	East Antarctic	Fast ice	43-10385	121-31372	1-307	
Lee et al.	2017	>0.8 µm	Eastern tropical S.Pacific	All	bdl-159	bdl-162	bdl-8.7	bdl-983
Marsay et al.	2017	>0.4 µm	Ross Sea	All	0.68-57.3	ND-185	ND-1.4	5.4-404
Milne et al.	2017	>0.45µm	Sub-tropical N.A.	All	ND-140	ND-800		
Ohnemus et al.	2015	0.8–51 µm	N. Atlantic	All	0-938	0-3600		
Planquette et al.	2009	>53 µm	Southern Ocean	30-340	0.15–13.2	0.11–25.5		
Schlosser et al.	2017	>1 µm	South Georgia Shelf	All	0.87-267	0.6-195	0.01-3.85	
Sherrell et al.	1998	1-53um	Northeast Pacific	0-3557		0.0-54.2		
Weinstein et al.	2004	>53 µm	Labrador Sea	0-250	0.1-1.2	0.1-1.5		
Weinstein et al.	2004	0.4– 10um	Labrador Sea	0-250	2.5	3.6	0.05	
Weinstein et al.	2004	>0.4 µm	Gulf of Maine	0-300	34.8	109		

Table 2: Concentration (in nmol L^{-1}) of trace elements (PFe, Pal, PMn and PP) in suspended particles collected in diverse regions of the world's ocean. Bdl: below detection limit, ND: non-determined.